for 1 h. First antibody was polyclonal guinea pig anti-glial fibrillary acidic protein (GFAP) (1 : 400 dilution) (Progen, Germany) at 4°C overnight, while negative control sections were incubated without primary antibody. Secondary antibody was goat anti-guinea pig biotin conjugate (1 : 400 dilution) (Sigma) for 1 h at room temperature, and was followed by streptavidin-coupled horseradish peroxidase complex (Vector Laboratories; 1 : 200 dilution) for 1 h. After extensive washing, sections were developed under identical conditions for all specimens with 3,3-diaminobenzidine tetrahydrochloride (Sigma–Aldrich) in 0.1 M phosphate buffer until a clear dark-brown labelling of astrocytes in the gracile tract could be detected. In all cases the control sections without primary antibody incubation showed no labelling of astrocytes. For microscopic examination and TV densitometry, sections were dehydrated and mounted in Entellan resin (Merck). Quantitation was similar to that described for Luxol Fast Blue densitometry. GFAP immunostaining intensities in cranial gracile tract sections were expressed as percentage of GFAP staining intensity in wild-type sections at the same coronal level. We applied GFAP densitometry on representative cranial gracile tract sections from each examined mouse: two sections from level C2/C3 representing the cervical gracile fascicle and two sections from level 535 representing the gracile nucleus (Sidman *et al.*, 1971).

Immunocytochemistry of sciatic nerves

Sciatic nerves from 15-week-old *gad*, *gad*/*Wld*^{S}, or control mice were immersion fixed in 4% PFA/0.1 M PBS for 1 h and washed extensively in 0.1 M PBS before paraffin embedding. Twenty-micrometre sections were immunostained using rabbit polyclonal antibody to ubiquitin (Sigma–Aldrich U5379) and Cy3-conjugated secondary antibody. Confocal images were obtained using a PerkinElmer UltraView LCI confocal microscope coupled to a Nikon Eclipse TE200 microscope, and processed using UltraView software (Perkin-Elmer Life Sciences Ltd, Cambridge, UK).

Statistical analysis of histopathology results

All data (axonal spheroid numbers, TV densitometry intensities) are presented as mean ± SD for the examined genotype groups. Data analysis was performed using PRISM for Macintosh or SPSS for Windows, including Student's *t*-test calculations for paired and unpaired data where appropriate. Significance was considered at $P < 0.05$ and high significance at a $P < 0.01$.

Analysis of neuromuscular pathology

Mice were killed by cervical dislocation and lumbrical muscles immediately dissected under oxygenated Ringer solution. Fixation, immunocytochemistry and signal imaging were then carried out as described previously (Gillingwater *et al.*, 2002). The denervation rate was determined by counting 100–200 endplates in each of two to three lumbrical muscles and the mean value taken for each mouse.

Behavioural tests

The foot splay test (Norreel *et al.*, 2001) was used to estimate the reflex reaction speed of the hind limbs. Mice were gently taken by the neck and tail, the plantar surface of their hind feet painted using a non-toxic children's painting set, and the mouse released from a height of 15 cm to land on white paper. Wild-type mice bring their legs together during descent to land in a controlled manner like a gymnast, whereas *gad* mice fail to do this and land with their feet far apart. The distance between the two hind heels was averaged from 10 successive trials on each testing date (9 and 13 weeks).

In the clasping test, the mouse was suspended by the tail >50 cm from any surface. Clasping time within a 1 min test was scored as flexing or folding of the hind limbs tightly towards the trunk plus any spasmodic stretching. Mice were examined once per week through the period from 6 to 16 weeks. No wild-type mice clasped, regardless of the presence of the *Wld*^{S} mutation.

Results

gad does not weaken the Wld^S *phenotype*

Before assessing the effect of *Wld*^{S} on *gad* pathology we first showed that *Wld*^{S} can protect axons, even in the presence of the *gad* mutation, by inducing Wallerian degeneration in *gad*/*Wld*^{S} mice. Before the lesion, there was no sign of axon degeneration in these nerves, confirming previous reports (Mukoyama *et al.*, 1989). We bred *gad* mice that were heterozygous for *Wld*^{S} and hemizygous for a *YFP-H* transgene (Feng *et al.*, 2000) to allow a rapid and quantitative assessment of Wallerian degeneration (Beirowski *et al.*, 2004) and transected sciatic nerves before the onset of hindlimb weakness. Wallerian degeneration was assessed after 5 days both by western blotting to see degraded heavy neurofilament protein (Fig. 1A) and by fluorescence microscopy to see fragmented YFP-containing axons (Fig. 1B). Nerves unprotected by *Wld*^{S} degenerated as expected (Fig. 1A, middle lane, and Fig. 1B, lower panel) but a single allele of *Wld*^{S} was sufficient to prevent axon degeneration in both readout methods. Thus, *gad* does not significantly weaken the *Wld*^{S} phenotype and it is feasible to test the effect of *Wld*^{S} on *gad* pathology.

Axonal spheroid pathology is reduced by Wld^S

In order to determine the effectiveness of *Wld*^{S} on *gad* axonal spheroid pathology, we counted axonal spheroids in ~90 H & E stained 6-μm paraffin sections from throughout the gracile nucleus and 30 sections from throughout the cervical spinal cord of each 18-week-old *gad* mouse and *gad*/*Wld*^{S} double homozygote. Fifty per cent fewer spheroids were found in gracile nuclei of *gad*/*Wld*^{S} mice than in *gad* mice ($P = 0.0004$) and 63% fewer in cervical gracile fascicle ($P = 0.0011$) (Fig. 2). Intermediate values were observed in *Wld*^{S} heterozygotes, further supporting the result and no spheroids were observed in control animals of this age (data not shown). Spheroids have also been reported in the cervical lateral columns of *gad* mice (Kikuchi *et al.*, 1990). We found far fewer spheroids here than in cervical gracile tract and gracile nucleus, but the number was also significantly reduced by homozygous *Wld*^{S} ($P = 0.046$; $n = 3$) (Fig. 2). We also observed a reduction in axonal spheroids in lumbar spinal cord, from 42 to six in the ventral column and from 13 to four

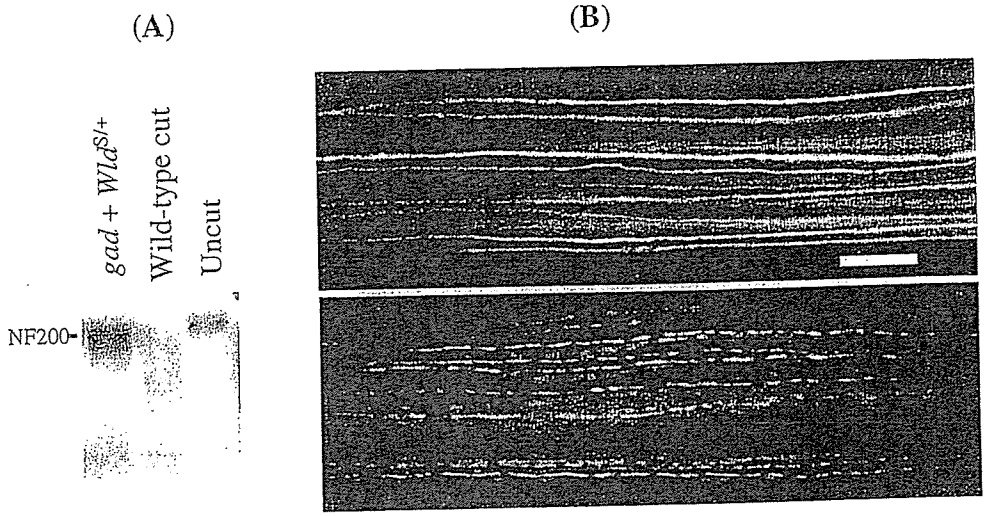

Fig. 1 A single allele of Wld^S is sufficient to delay Wallerian degeneration even in *gad* mice. (**A**) Western blot showing complete preservation of intact heavy neurofilament protein (NF200) in the distal stump of axotomized *gad* sciatic nerve by heterozygous Wld^S 5 days after lesion (lane 1). In contrast, no intact NF200 remains after 5 days in axotomized wild-type sciatic nerve (lane 2). Lane 3 is an uncut nerve showing the expected appearance of intact NF200 (gel loading differences probably account for the difference in intensity with lane 1). (**B**) Complete preservation of distal *gad* tibial nerve by heterozygous Wld^S 5 days after nerve lesion (upper panel), visualized using the *YFP-H* transgene. In contrast, no unfragmented axons remained in a tibial nerve lacking Wld^S 3 days after a lesion (lower panel). Unlesioned nerves appear exactly as in the upper image (Beirowski *et al.*, 2004). Scale bar = 100 μm.

in the dorsal horn grey matter. Although lumbar regions of only a single *gad* and two *gad*/Wld^S mice were studied, these mice were independent of those used for the gracile tract analysis and 3 weeks younger, so these data independently support our conclusion that Wld^S reduces axonal spheroid pathology in several different regions of *gad* CNS well into late-stage disease.

A reduction in the number of axonal spheroids could result theoretically from either reduced axon pathology or pathology so extensive that the axons are completely destroyed. Kurihara *et al.* (2001) reported that when *gad* pathology was made worse by crossing with *Uch-l3* null mice, extensive axon pathology became detectable at more caudal locations in cervical and thoracic gracile fascicle. We did not observe this in the Wld^S cross, and Wld^S homozygotes maintain a rostral–caudal gradient of axonal spheroid pathology (Fig. 2E and F; and thoracic data not shown), indicating that *gad* remains a 'dying-back' pathology in Wld^S mice but that its progress is delayed.

Secondary measures of axon pathology are also reduced by Wld^S

Further evidence of a reduced loss of axon-myelin units in *gad*/Wld^S mice came from a significant reduction ($P = 0.018$) in secondary myelin loss in cervical gracile fascicle in the same animals (Fig. 3A–C). A similar protective trend in the medulla oblongata did not reach statistical significance ($P = 0.059$), probably due to the naturally weaker myelination in this region, but Wld^S clearly did not cause any deterioration, so the reduction in axonal spheroid numbers (Fig. 2) must reflect reduced pathology and not wholesale axon loss. Furthermore, as the rescued axons remain myelinated, they potentially retain normal conductance properties, at least in these locations. It is unlikely that Wld^S has any direct effect on myelin, because expression of Wld^S in glia does not alter Wallerian degeneration (Glass *et al.*, 1993). Thus reduced myelin loss in *gad*/Wld^S mice is likely to reflect the maintenance of functional axon-myelin units. Wld^S also decreased GFAP signal in immunocytochemistry in *gad*, indicating a lower level of astrocyte activation in response to axon damage (Yamazaki *et al.*, 1988) (data not shown). Thus, both direct and indirect measures of spheroidal axon pathology in the gracile tract are reduced by the Wld^S gene.

Wld^S operates downstream of axonal ubiquitin depletion in gad

gad causes axon degeneration through defective ubiquitin metabolism (Osaka *et al.*, 2003), and Wld^S also interferes with ubiquitin metabolism (Mack *et al.*, 2001; Coleman and Perry, 2002; Zhai *et al.*, 2003). It was important to establish whether Wld^S blocks the ubiquitin defect in *gad*, an action that would suggest a protective effect restricted to *gad* and other ubiquitin defects, or whether it acts on a downstream step, raising the possibility of delaying axonal spheroid pathology in a wide range of CNS disorders (see above). Interpretation of any change in ubiquitin level in gracile tract would be complicated by the degeneration of those axon branches, so instead we carried out immunocytochemistry for ubiquitin epitopes in the peripheral branch of the same axons in sciatic nerve (Fig. 4). First, we confirmed that axonal ubiquitin was severely depleted in *gad* mice compared with wild-type controls ($P = 0.014$) (Osaka *et al.*, 2003). We then found

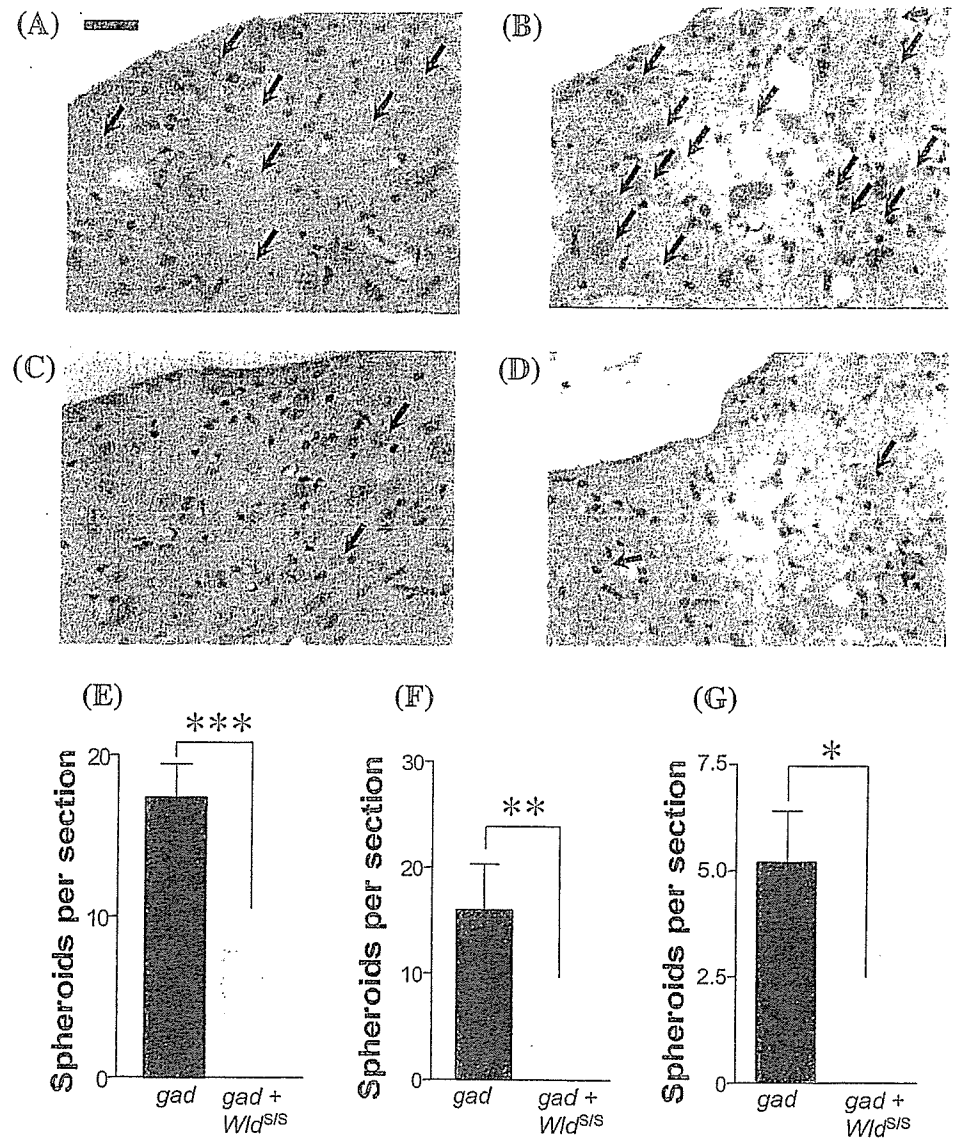

Fig. 2 *Wld*^{S} reduces spheroid body numbers in the gracile tract and lateral columns of *gad* mice. (**A** and **C**) Representative sections from gracile nucleus of (**A**) *gad* and (**C**) *gad/Wld*^{S} mice stained with H & E, showing a large reduction in the number of axonal spheroids (large pink swellings, indicated by arrows) when *Wld*^{S} is present. (**B** and **D**) Representative sections from cervical gracile fascicle of (**B**) *gad* and (**D**) *gad/Wld*^{S} mice. Scale bar (**A**–**D**) = 25 μm. (**E**–**G**) Quantitation (mean ± SD) of spheroid counting data in (**E**) gracile nucleus (n = 6), (**F**) cervical gracile fascicle (n = 6) and (**G**) cervical lateral columns (n = 3). *$P < 0.05$; **$P < 0.01$; ***$P < 0.001$.

that a similar defect was present in *gad/Wld*^{S} mice compared with *Wld*^{S} controls (P = 0.0004) and that *Wld*^{S} did not significantly increase the ubiquitin signal either in the presence (P = 0.902) or absence (P = 0.807) of *gad*. Thus, *Wld*^{S} does not correct the depletion of axonal ubiquitin in *gad* and instead operates at a downstream point in spheroid pathology that could be common to other CNS disorders.

Motor pathology

Despite the reduction in axonal spheroids in the gracile tract, there was no apparent reduction in the severity of *gad* symptoms when *Wld*^{S} was present, with no significant difference in hindlimb clasping, (P = 0.82; n = 9) or splay test (P = 0.33; n = 7). Thus, either prevention of swelling in the gracile tract does not preserve the function of those axons, or pathology elsewhere limits any improvement in phenotype of *gad/Wld*^{S} mice. In the absence of any tests to specifically target the function of gracile tract axons, we investigated neuromuscular junction (NMJ) pathology, where dying-back of motor nerve terminals has previously been reported (Miura *et al.*, 1993). At 15 weeks, the degree of denervation was similar between the two strains, with 56.0 ± 6.0% of lumbrical NMJ fully or partially denervated in *gad* mice and 53.5 ± 11.8% in *gad/Wld*^{S} (Fig. 5C and D). This may be because protection of motor nerve terminals at the NMJ by *Wld*^{S} after axotomy is weaker than that of the axon trunk, especially in older mice (Gillingwater *et al.*, 2002). However,

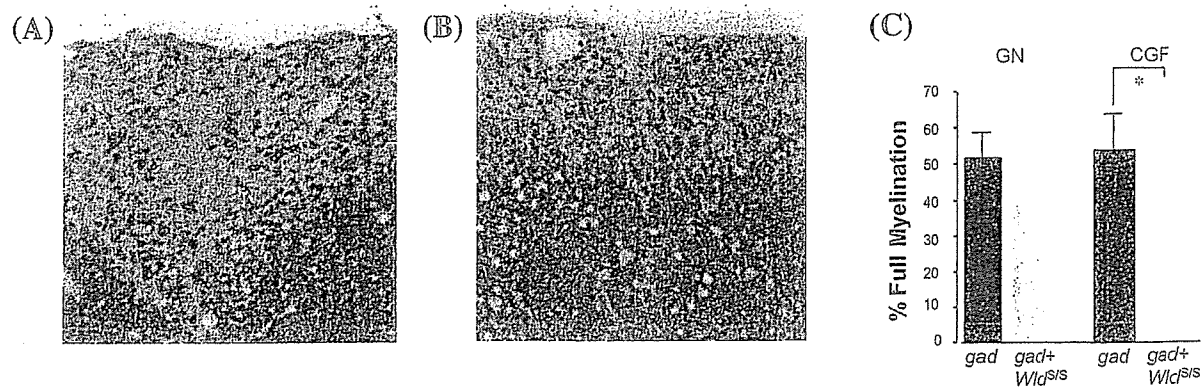

Fig. 3 *Wld*^{S} reduces also secondary demyelination in the gracile tract. (A and B) Representative cervical gracile fascicles of (A) *gad* and (B) *gad/Wld*^{S} mice stained with Luxol Fast Blue and Nuclear Fast Red, showing the reduction in myelin loss when *Wld*^{S} is present. Scale bar (A and B) = 25 μm. (C) Densitometric quantification (mean ± SD) of Luxol Fast Blue staining (n = 5). *P < 0.05.

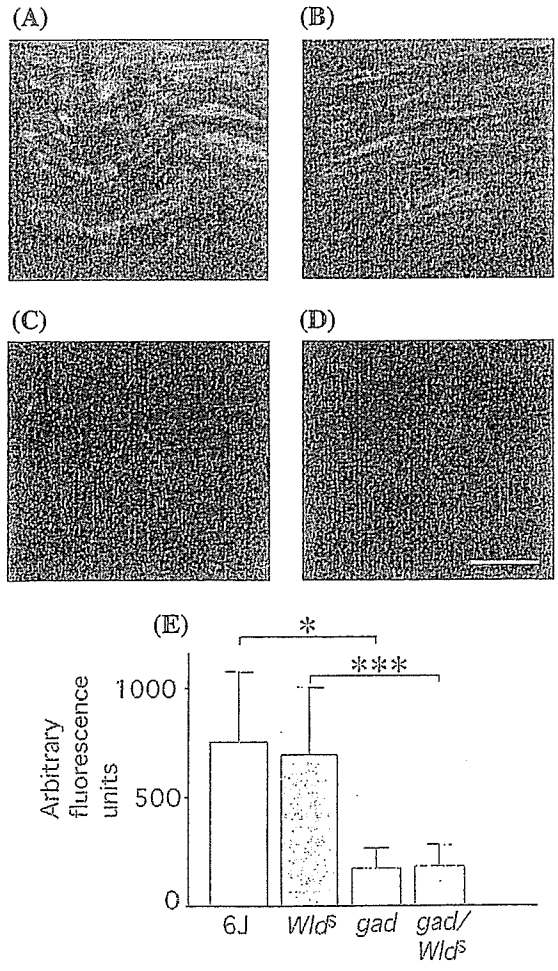

Fig. 4 *Wld*^{S} does not correct the severe depletion of axonal ubiquitin in *gad*. Ubiquitin immunostaining in both (A) wild-type and (B) *Wld*^{S} mice is greatly reduced in C and D, respectively, where *gad* is also present. Comparison of A with B and C with D also shows that *Wld*^{S} does not alter ubiquitin signal either in the presence of absence of *gad*. (E) Quantitation (mean ± SD) of ubiquitin signal. *P < 0.05; ***P < 0.001. 6 J, n = 4; *Wld*^{S}, n = 4; *gad*, n = 4; and *gad/Wld*^{S}, n = 10. Scale bar = 50 μm.

at 9 weeks, an age where *Wld*^{S} does protect axotomized motor nerve terminals, neither strain showed any denervation of NMJ in lumbrical muscles (Fig. 5A and B), so there was no time window when both *Wld*^{S} and *gad* exert their opposing effects at the NMJ. Thus, the fact that *Wld*^{S} does not alleviate NMJ pathology in the older mice could explain why *gad* symptoms are not reduced.

Discussion

We report that *Wld*^{S} reduces the occurrence of axonal spheroids in *gad*. This is the first indication that *Wld*^{S} can alleviate axon pathology in chronic CNS disease, thus extending observations made in the PNS that *Wld*^{S} protects axons not only after injury (Lunn *et al.*, 1989) but also in disorders where no physical injury takes place (Wang *et al.*, 2002; Ferri *et al.*, 2003; Samsam *et al.*, 2003). We conclude that axonal spheroid pathology in *gad* and Wallerian degeneration are not independent events and axon degeneration mechanisms are more uniform than morphology would suggest. It follows that Wallerian degeneration, or processes related to it, could contribute to many other CNS disorders where its involvement has not previously been suspected.

The mechanism by which *Wld*^{S} protects axons is still under investigation (Mack *et al.*, 2001; Coleman and Perry, 2002; Zhai *et al.*, 2003; Araki *et al.*, 2004), but appears to involve nuclear Wld^S protein and a factor(s) that communicates its effect to the axon. What is already becoming clear, however, is that *Wld*^{S} directly or indirectly blocks a central step of axon pathology onto which various pathological mechanisms converge (Fig. 6). This is indicated both by the wide range of disorders in which *Wld*^{S} protects axons, as it is inconceivable that *Wld*^{S} blocks different initial events in each case, and by our direct evidence, that early steps of *gad* pathogenesis are unaltered (Fig. 4). Intriguingly, it now seems that a number of different pathological manifestations result from the step delayed by *Wld*^{S}. These are axonal spheroids in *gad*, dying-back axon loss without swelling in peripheral

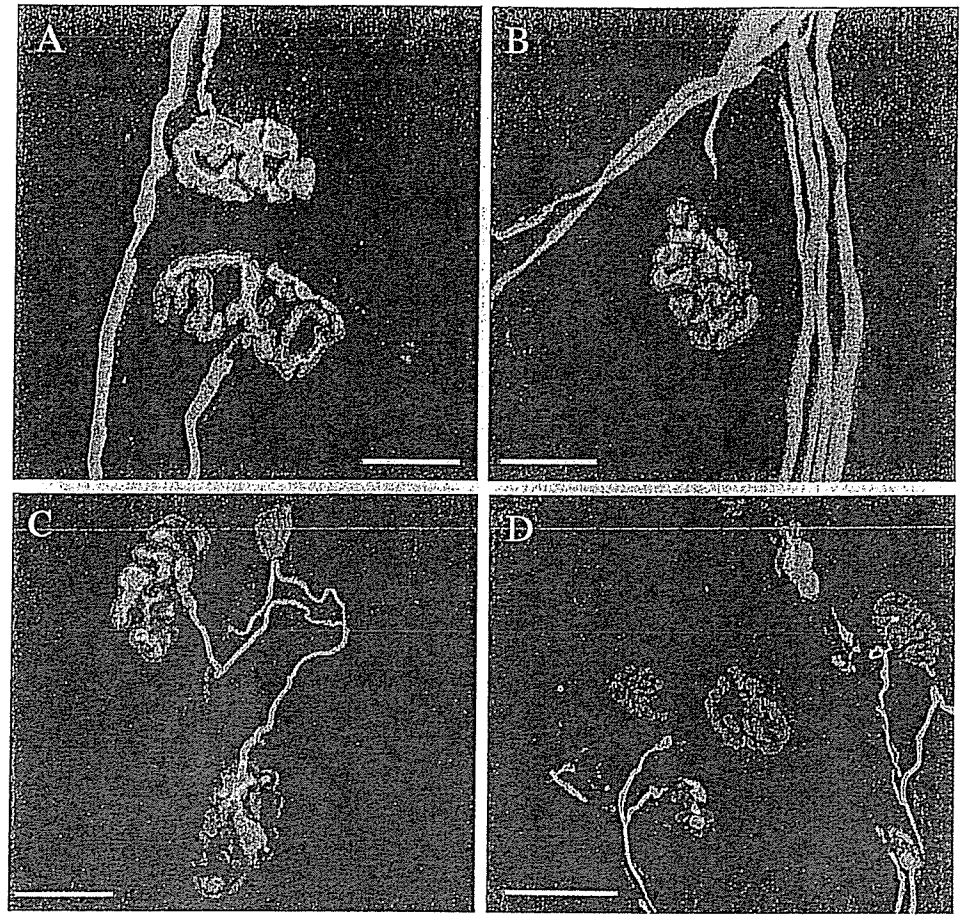

Fig. 5 Denervation at the NMJ. Presynaptic structures labelled with SV2 and neurofilament antibody are shown in green, and postsynaptic structures labelled with TRITC-α-bungarotoxin are in red. At 9 weeks, denervation has hardly begun in (**A**) *gad* or (**B**) *gad*/*Wld*^{S}. At 15 weeks, both strains show extensive denervation (**C** and **D**, respectively), with partial occupancy of endplates by motor nerve terminals occurring frequently. Scale bar = 25 μm.

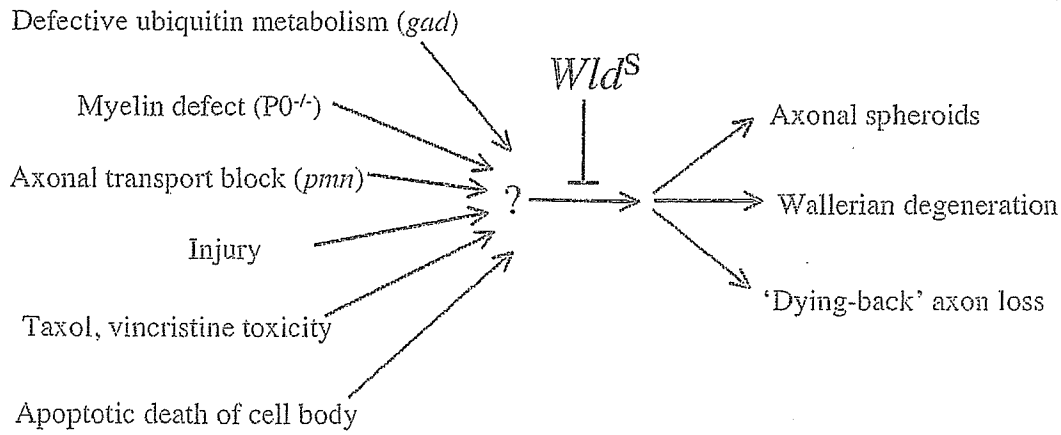

Fig. 6 *Wld*^{S} delays a central step of axonal pathology that lies after the convergence point of multiple degenerative stimuli but upstream of the divergence of several pathological manifestations.

neuropathy and motor neuronopathy, and Wallerian degeneration in CNS and PNS injury. The divergent morphology and topology in these disorders previously suggested independent mechanisms, but the results of directly probing the mechanism using *Wld*^{S} challenge this interpretation.

Many CNS disorders in which there is axonal swelling show accumulation of amyloid precursor protein in the swellings,

indicating impairment of axonal transport in each case and suggesting that their axon degeneration mechanisms are to some extent related. *gad* is one of these disorders, and the others include brain trauma (Gentleman *et al.*, 1993), stroke (Dewar *et al.*, 1999) and other forms of ischaemia (Hughes *et al.*, 2003), multiple sclerosis (Ferguson *et al.*, 1997), and HIV dementia (Medana and Esiri; 2003). This similarity with *gad* suggests that axon degeneration in other disorders may also be related to Wallerian degeneration, a possibility that should now be tested using Wld^S mice or, where appropriate, the newly generated Wld^S rat model (Adalbert *et al.*, in press). However, it is unlikely that Wld^S will stop all forms of axonal swelling, as it appears unable to do so in *Plp* null mice (Edgar *et al.*, 2004). Thus, it should be possible to categorize CNS axonal swelling disorders into those that are altered by Wld^S and those that are not. This will then enable disorders to be grouped together for mechanistic studies rather than focusing on each disorder in isolation.

It is important to consider the spatial and temporal relationship between axonal swelling and axonal breakdown in the light of our data. The lack of good methods for longitudinal imaging of CNS axons has made it difficult to determine whether spheroids first occur as terminal endbulbs of axons whose distal ends have degenerated, or as localized swellings on otherwise morphologically normal axons. Preliminary data from our laboratory using axons of *gad*/YFP-H mice (Adalbert and Coleman., unpublished) suggest that many spheroids in *gad* are not terminal endbulbs, at least in the early stages of the disease. Thus, one model to account for the effect of Wld^S in *gad* is that an 'en passant' spheroid is the first step in pathology, leading to degeneration of the distal axon due to the blockage of axonal transport, a process that fixes the spheroid as a terminal endbulb. In this model, Wld^S might block the Wallerian-like degeneration of the distal end for long enough to allow the spheroid to resolve and the axon to recover. Thus, our data suggest that Wld^S could be used to address the question of whether swollen axons can recover or whether they are destined, inevitably, to degenerate. In a wider context, this is an important issue in several CNS disorders where axonal spheroids occur, including brain trauma and multiple sclerosis (Cheng and Povlishock, 1988; Ferguson *et al.*, 1997).

The above model assumes that Wallerian-like degeneration and axonal swelling in *gad* are separated in space and time, with one causing the other. Alternatively, the mechanism of the axonal swelling itself in *gad* may be related to that of Wallerian degeneration. In support of this model, there are a number of disorders in which CNS axons swell and PNS axons of the same animal degenerate by Wallerian-like degeneration without extensive swelling. In *gad* mice, this occurs even within the same cell, as gracile tract central projections of lumbar primary sensory neurons have spheroids, while peripheral muscle spindles degenerate without swelling (Oda *et al.*, 1992). Similarly, amyotrophic lateral sclerosis (ALS) in humans (Tu *et al.*, 1996; Takahashi *et al.*, 1997), mice (Tu *et al.*, 1996; Oosthuyse *et al.*, 2001) and rats (Howland *et al.*, 2002), together with tauopathy in mice (Lewis *et al.*, 2000; Probst *et al.*, 2000), all show axonal swelling in spinal cord and other CNS areas, but extensive 'Wallerian-like' degeneration without swelling in ventral roots and peripheral nerves. Even injury-induced Wallerian degeneration shows different morphology depending on experimental circumstances. For example, when injured gracile tract axons undergo Wallerian degeneration they swell to up to 10 times their normal diameter, quite unlike Wallerian degeneration in the PNS (George and Griffin, 1994). Thus, a number of observations support a direct mechanistic link between axonal swelling and Wallerian degeneration.

It is not yet clear how related mechanisms might cause swelling in spheroids but axon fragmentation in Wallerian degeneration. Cytoskeletal changes are common to both, so a loosening of cytoskeletal structure could cause disorganized cytoskeleton to accumulate in spheroids but to undergo rapid granular disintegration in Wallerian degeneration. Wallerian degeneration of injured gracile tract axons displays elements of both processes, possibly having an intermediate mechanism: like spheroids, these axons dilate considerably but, typical of Wallerian degeneration, they also rapidly lose their cytoskeletal proteins (George and Griffin, 1994). In traumatic brain injury, observation of Wallerian degeneration and spheroids in the same transverse thin section has been interpreted as degenerating axons having a more proximal spheroid that blocks axonal transport (Cheng and Povlishock, 1988). In view of our findings, an additional explanation needs to be considered, that spheroids and Wallerian degeneration are alternative responses of different axons to the same lesion. Methods for real-time or long-range longitudinal analysis of individual spheroid-containing axons are required to resolve this, similar to new methods already applicable in PNS axons (Pan *et al.*, 2003; Beirowski *et al.*, 2004). What determines whether an axon develops a spheroid or undergoes Wallerian degeneration? Possible explanations include the different glial and haematopoietic cell content of the CNS and the lower rate of axonal transport there (Wujek and Lasek, 1983), but injury type may also be important. Finally, since the discovery of the Wld^S mouse, Wallerian degeneration is no longer considered a passive wasting of distal axons but a regulated self-destruction programme (Buckmaster *et al.*, 1995; Raff *et al.*, 2002). The reduction of axonal spheroid pathology in *gad* by the same gene raises similar questions: rather than being a passive consequence of blocked axonal transport axonal swelling could be, like Wallerian degeneration, a programmed response to axon damage.

Altered ubiquitin metabolism plays important roles in neurodegenerative diseases of the CNS. Genetic mutations in Parkinson's disease include an E3 ligase (Kitada *et al.*, 1998) and possibly *UCH-L1*, the human homologue of the gene mutated in *gad* (Leroy *et al.*, 1998). Ubiquitin-positive inclusions and other evidence indicate abnormal ubiquitylation in Alzheimer's disease (Mori *et al.*, 1987;

van Leeuwen *et al.*, 1998), polyglutamine disorders (DiFiglia *et al.*, 1997; Cummings *et al.*, 1999; Bence *et al.*, 2001) and ALS (Tu *et al.*, 1996; Bruijn *et al.*, 1997). Axons and synapses are particularly vulnerable, as proteasome inhibitors cause specific degeneration of distal neurites (Laser *et al.*, 2003) and ubiquitin-related mutations alter synapse growth (DiAntonio *et al.*, 2001) and stability (Wilson *et al.*, 2002). As *Wld*^{S} can counter a downstream effect of defective ubiquitin metabolism, it now becomes important to study its effects on the above disorders.

Wld^S did not alleviate the symptoms of *gad* mice. Unfortunately, methods do not currently exist to assess the function of gracile tract axons, so we cannot rule out the possibility that blocking spheroid formation did not preserve axon function. However, it is likely that continued neuromuscular pathology in *gad/Wld*^{S} mice also contributes to the symptoms. These mice suffered extensive synapse loss by 15 weeks (Fig. 5), whereas axon pathology was still strongly reduced 3 weeks later (Fig. 2). This supports the hypothesis that different mechanisms underlie synaptic and axonal degeneration, with *Wld*^{S} affording only limited protection to synapses, particularly in older mice (Gillingwater and Ribchester, 2001; Gillingwater *et al.*, 2002). Similarly, the synapses of gracile tract axons may have been lost even when those axons are preserved. Our data suggest that synapse pathology is a limiting factor when axons are protected by *Wld*^{S}, a finding likely to be important in other models (Ferri *et al.*, 2003; Samsam *et al.*, 2003).

In summary, we conclude that *Wld*^{S} alleviates chronic CNS axon pathology in *gad* mice and that formation of distal axonal spheroids in this disease shares features with Wallerian degeneration and 'dying-back' axon loss without spheroids. The effect of *Wld*^{S} on other CNS disorders with ubiquitylation deficits and CNS axonal swelling disorders should now be studied. Finally, our data emphasize the importance of finding a way to protect synapses as strongly as *Wld*^{S} protects axons.

Acknowledgements

We thank Professor Tateki Kikuchi for advice on *gad* pathology, Professor Rudolf Martini (University of Würzburg), Dr Mohtashem Samsam (University of Würzburg and Saba University School of Medicine), Dr Till G. A. Mack (Key Neurotek, Magdeburg, Germany), Dr Martin Bootman (The Babraham Institute, Cambridge) and Ms Jolanta Kozlowski (University of Cologne) for helpful discussion and technical advice. This work was supported by the Federal Ministry of Education and Research (FKZ: 01 KS 9502) and Center for Molecular Medicine, University of Cologne (CMMC) (to W.M., B.B., R.A., D.W., D.G. and M.P.C.), the Wellcome Trust (to T.H.G., plus Biomedical Collaboration Grant to R.R.R. and M.P.C), the Biotechnology and Biological Sciences Research Council (M.P.C., R.A., L.C.), ALSA (R.A.), the Koeln Fortune Programme (B.B.), the Grants-in-Aid for Scientific Research from the Ministry of Education, Culture, Sports, Science and Technology of Japan (K.W.) and from the Ministry of Health, Labour and Welfare of Japan (K.W.).

References

Adelbert R, Gillingwater TM, Haley JE, Bridge K, Beirowski B, Berek L, Wagner D, Grumme D, Thomson D, Celik A, Addicks K, Ribchester RR, and Coleman MP. A rat model of slow Wallerian degeneration (Wld^S) with improved preservation of synapses. Eur J Neurosci. In press.

Adle-Biassette H, Chretien F, Wingertsmann L, Hery C, Ereau T, Scaravilli F, et al. Neuronal apoptosis does not correlate with dementia in HIV infection but is related to microglial activation and axonal damage. Neuropathol Appl Neurobiol 1999; 25: 123–33.

Araki T, Sasaki Y, Milbrandt H. Increase nuclear NAD biosynthesis and SIRT1 activation prevent axonal degeneration. Science 2004; 305: 1010–3.

Beirowski B, Berek L, Adalbert R, Wagner D, Grumme DS, Addicks K, et al. Quantitative and qualitative analysis of Wallerian degeneration using restricted axonal labeling in YFP-H mice. J Neurosci Methods 2004; 134: 23–35.

Bence NF, Sampat RM, Kopito RR. Impairment of the ubiquitin–proteasome system by protein aggregation. Science 2001; 292: 1552–5.

Bomont P, Cavalier L, Blondeau F, Ben Hamida C, Belal S, Tazir M, et al. The gene encoding gigaxonin, a new member of the cytoskeletal BTB/kelch repeat family, is mutated in giant axonal neuropathy. Nat Genet 2000; 26: 370–4.

Brendza RP, O'Brien C, Simmons K, McKeel DW, Bales KR, Paul SM, et al. PDAPP;YFP double transgenic mice: a tool to study amyloid-b associated changes in axonal, dendritic and synaptic structures. J Comp Neurol 2003; 456: 375–83.

Bruijn LI, Becher MW, Lee MK, Anderson KL, Jenkins NA, Copeland NG, et al. ALS-linked SOD1 mutant G85R mediates damage to astrocytes and promotes rapidly progressive disease with SOD1-containing inclusions. Neuron 1997; 18: 327–38.

Bu B, Li J, Davies P, Vincent I. Deregulation of cdk5, hyperphosphorylation, and cytoskeletal pathology in the Niemann–Pick Type C murine model. J Neurosci 2002; 22: 6515–25.

Buckmaster EA, Perry VH, Brown MC. The rate of Wallerian degeneration in cultured neurons from wild type and C57BL/Wld^S mice depends on time in culture and may be extended in the presence of elevated K^+ levels. Eur J Neurosci 1995; 7: 1596–602.

Cheng CLY, Povlishock JT. The effect of traumatic brain injury on the visual system: a morphologic characterization of reactive axonal change. J Neurotrauma 1988; 5: 47–60.

Coleman MP, Perry VH. Axon pathology in neurological disease: a neglected therapeutic target. Trends Neurosci 2002; 25: 532–7.

Coleman MP, Conforti L, Buckmaster EA, Tarlton A, Ewing RM, Brown MC, et al. An 85-kb tandem triplication in the slow Wallerian degeneration (Wld^S) mouse. Proc Natl Acad Sci USA 1998; 95: 9985–90.

Conforti L, Tarlton A, Mack TG, Mi W, Buckmaster EA, Wagner D, et al. A Ufd2/D4Cole1e chimeric protein and overexpression of Rbp7 in the slow Wallerian degeneration (Wld^S) mouse. Proc Natl Acad Sci USA 2000; 97: 11377–82.

Cummings CJ, Reinstein E, Sun Y, Antalffy B, Jiang Y, Ciechanover A, et al. Mutation of the E6-AP ubiquitin ligase reduces nuclear inclusion frequency while accelerating polyglutamine-induced pathology in SCA1 mice. Neuron 1999; 24: 879–92.

Dewar D, Yam P, McCulloch J. Drug development for stroke: importance of protecting cerebral white matter. Eur J Pharmacol 1999; 375: 41–50.

DiAntonio A, Haghighi AP, Portman SL, Lee JD, Amaranto AM, Goodman CS. Ubiquitination-dependent mechanisms regulate synaptic growth and function. Nature 2001; 412: 449–52.

DiFiglia M, Sapp E, Chase KO, Davies SW, Bates GP, Vonsattel JP, et al. Aggregation of huntingtin in neuronal intranuclear inclusions and dystrophic neurites in brain. Science 1997; 277: 1990–3.

Edgar JM, McLaughlin M, Yool D, Zhang SC, Fowler JH, Montague P, et al. Oligodendroglial modulation of fast axonal transport in a mouse model of hereditary spastic paraplegia. J Cell Biol 2004; 166: 121–31.

Feng G, Mellor RH, Bernstein M, Keller-Peck C, Nguyen QT, Wallace M, et al. Imaging neuronal subsets in transgenic mice expressing multiple spectral variants of GFP. Neuron 2000; 28: 41–51.

Ferguson B, Matyszak MK, Esiri MM, Perry VH. Axonal damage in acute multiple sclerosis lesions. Brain 1997; 120: 393–9.

Ferreirinha F, Quattrini A, Pirozzi M, Valsecchi V, Dina G, Broccoli V, et al. Axonal degeneration in paraplegin-deficient mice is associated with abnormal mitochondria and impairment of axonal transport. J Clin Invest 2004; 113: 231–42.

Ferri A, Sanes JR, Coleman MP, Cunningham JM, Kato AC. Inhibiting axon degeneration and synapse loss attenuates apoptosis and disease progression in a mouse model of motoneuron disease. Curr Biol 2003; 13: 1–20.

Galvin JE, Uryu K, Lee VM, Trojanowski JQ. Axon pathology in Parkinson's disease and Lewy body dementia contains alpha-, beta-, and gamma-synuclein. Proc Natl Acad Sci USA 1999; 96: 13450–5.

Gentleman SM, Nash MJ, Sweeting CJ, Graham DI, Roberts GW. Beta-amyloid precursor protein (beta APP) as a marker for axonal injury after head injury. Neurosci Lett 1993; 160: 139–44.

George R, Griffin JW. The proximo-distal spread of axonal degeneration in the dorsal columns of the rat. J Neurocytol 1994; 23: 657–67.

Gillingwater TH, Ribchester RR. Compartmental neurodegeneration and synaptic plasticity in the Wld^S mutant mouse. J Physiol 2001; 534: 627–39.

Gillingwater TH, Thomson D, Mack TG, Soffin EM, Mattison RJ, Coleman MP, et al. Age-dependent synapse withdrawal at axotomised neuromuscular junctions in Wld^S mutant and Ube4b/Nmnat transgenic mice. J Physiol 2002; 543: 739–55.

Gillingwater TH, Haley JE, Ribchester RR, Horsburgh K. Neuroprotection after transient global cerebral ischemia in Wld(s) mutant mice. J Cereb Blood Flow Metab 2004; 24: 62–6.

Glass JD, Brushart TM, George EB, Griffin JW. Prolonged survival of transected nerve fibres in C57BL/Ola mice is an intrinsic characteristic of the axon. J Neurocytol 1993; 22: 311–21.

Griffiths I, Klugmann M, Anderson T, Yool D, Thomson C, Schwab MH, et al. Axonal swellings and degeneration in mice lacking the major proteolipid of myelin. Science 1998; 280: 1610–3.

Howland DS, Liu J, She Y, Goad B, Maragakis NJ, Kim B, et al. Focal loss of the glutamate transporter EAAT2 in a transgenic rat model of SOD1 mutant-mediated amyotrophic lateral sclerosis (ALS). Proc Natl Acad Sci USA 2002; 99: 1604–9.

Hughes PM, Anthony DC, Ruddin M, Botham MS, Rankine EL, Sablone M, et al. Focal lesions in the rat central nervous system induced by endothelin-1. J Neuropathol Exp Neurol 2003; 62: 1276–86.

Ichihara N, Wu J, Chui DH, Yamazaki K, Wakabayashi T, Kikuchi T. Axonal degeneration promotes abnormal accumulation of amyloid beta-protein in ascending gracile tract of gracile axonal dystrophy (GAD) mouse. Brain Res 1995; 695: 173–8.

Kikuchi T, Mukoyama M, Yamazaki K, Moriya H. Axonal degeneration of ascending sensory neurons in gracile axonal dystrophy mutant mouse. Acta Neuropathol (Berl) 1990; 80: 145–51.

Kitada T, Asakawa S, Hattori N, Matsumino H, Yamamura Y, Minoshima S, et al. Mutations in the parkin gene cause autosomal recessive juvenile parkinsonism. Nature 1998; 392: 605–8.

Kornek B, Storch MK, Weissert R, Wallstroem E, Stefferl A, Olsson T, et al. Multiple sclerosis and chronic autoimmune encephalomyelitis: a comparative quantitative study of axonal injury in active, inactive, and remyelinated lesions. Am J Pathol 2000; 157: 267–76.

Kornek B, Storch MK, Bauer J, Djamshidian A, Weissert R, Wallstroem E, et al. Distribution of a calcium channel subunit in dystrophic axons in multiple sclerosis and experimental autoimmune encephalomyelitis. Brain 2001; 124: 1114–24.

Kurihara LJ, Kikuchi T, Wada K, Tilghman SM. Loss of Uch-L1 and Uch-L3 leads to neurodegeneration, posterior paralysis and dysphagia. Hum Mol Genet 2001; 10: 1963–70.

Laser H, Mack TGA, Wagner D, Coleman MP. Proteasome inhibition arrests neurite outgrowth and causes 'dying-back' degeneration in primary culture. J Neurosci Res 2003; 15: 906–16.

Leroy E, Boyer R, Auburger G, Leube B, Ulm G, Mezey E, et al. The ubiquitin pathway in Parkinson's disease. Nature 1998; 395: 451–2.

Lewis J, McGowan E, Rockwood J, Melrose H, Nacharaju P, Van Slegtenhorst M, et al. Neurofibrillary tangles, amyotrophy and progressive motor disturbance in mice expressing mutant (P301L) tau protein. Nat Genet 2000; 25: 402–5.

Liberski PP, Budka H. Neuroaxonal pathology in Creutzfeldt–Jakob disease. Acta Neuropathol (Berl) 1999; 97: 329–34.

Lunn ER, Perry VH, Brown MC, Rosen H, Gordon S. Absence of Wallerian degeneration does not hinder regeneration in peripheral nerve. Eur J Neurosci 1989; 1: 27–33.

Mack TG, Reiner M, Beirowski B, Mi W, Emanuelli M, Wagner D, et al. Wallerian degeneration of injured axons and synapses is delayed by a Ube4b/Nmnat chimeric gene. Nat Neurosci 2001; 4: 1199–206.

Medana IM, Esiri MM. Axonal damage: a key predictor of outcome in human CNS diseases. Brain 2003; 126: 515–30.

Mi W, Conforti L, Coleman MP. Genotyping methods to detect a unique neuroprotective factor (Wld^S) for axons. J Neurosci Methods 2002; 113: 215–8.

Mi W, Glass JDG, Coleman MP. Stable inheritance of an 85-kb triplication in C57BL/Wld^S mice. Mut Res 2003; 526: 33–7.

Miike T, Ohtani Y, Nishiyama S, Matsuda I. Pathology of skeletal muscle and intramuscular nerves in infantile neuroaxonal dystrophy. Acta Neuropathol (Berl) 1986; 69: 117–23.

Miura H, Oda K, Endo C, Yamazaki K, Shibasaki H, Kikuchi T. Progressive degeneration of motor nerve terminals in gad mutant mouse with hereditary sensory axonopathy. Neuropathol Appl Neurobiol 1993; 19: 41–51.

Mori H, Kondo J, Ihara Y. Ubiquitin is a component of paired helical filaments in Alzheimer's disease. Science 1987; 235: 1641–4.

Mukoyama M, Yamazaki K, Kikuchi T, Tomita T. Neuropathology of gracile axonal dystrophy (gad) mouse. Acta Neuropathol 1989; 79: 294–9.

Norreel JC, Jamon M, Riviere G, Passage E, Fontes M, Clarac F. Behavioural profiling of a murine Charcot–Marie–Tooth disease type 1A model. Eur J Neurosci 2001; 13: 1625–34.

Oda K, Yamazaki K, Miura H, Shibasaki H, Kikuchi T. Dying back type axonal degeneration of sensory nerve terminals in muscle spindles of the gracile axonal dystrophy (gad) mutant mouse. Neuropathol Appl Neurobiol 1992; 18: 265–81.

Oosthuyse B, Moons L, Storkebaum E, Beck H, Nuyens D, Brusselmans K, et al. Deletion of the hypoxia-response element in the vascular endothelial growth factor promoter causes motor neuron degeneration. Nat Genet 2001; 28: 131–8.

Osaka H, Wang Y-L, Takada K, Takizawa S, Setsuie R, Li H, et al. Ubiquitin carboxy-terminal hydrolase L1 binds to and stabilises monoubiquitin in neurons. Hum Mol Genet 2003; 12: 1945–58.

Pan YA, Misgeld T, Lichtman JW, Sanes JR. Effects of neurotoxic and neuroprotective agents on peripheral nerve regeneration assayed by time-lapse imaging *in vivo*. J Neurosci 2003; 23: 11479–88.

Probst A, Gotz J, Wiederhold KH, Tolnay M, Mistl C, Jaton AL, et al. Axonopathy and amyotrophy in mice transgenic for human four-repeat tau protein. Acta Neuropathol (Berl) 2000; 99: 469–81.

Raff MC, Whitmore AV, Finn JT. Axonal self-destruction and neurodegeneration. Science 2002; 296: 868–71.

Raja F, Sherriff FE, Morris CS, Bridges LR, Esiri MM. Cerebral white matter damage in HIV infection demonstrated using beta-amyloid precursor protein immunoreactivity. Acta Neuropathol (Berl) 1997; 93: 184–9.

Saigoh K, Wang YL, Suh JG, Yamanishi T, Sakai Y, Kiyosawa H, et al. Intragenic deletion in the gene encoding ubiquitin carboxy-terminal hydrolase in gad mice. Nat Genet 1999; 23: 47–51.

Sajadi A, Schneider BL, Aebischer P. Wld^S-mediated protection of dopaminergic fibers in an animal model of Parkinson disease. Curr Biol 2004; 14: 326–30.

Samsam M, Mi W, Wessig C, Zielasek J, Toyka KV, Coleman MP, et al. The Wld^S mutation delays robust loss of motor and sensory axons in a

genetic model for myelin-related axonopathy. J Neurosci 2003; 23: 2833–9.

Sidman RL, Angevine JB, Pierce ET. Atlas of mouse brain and spinal cord. Cambridge: Harvard University Press; 1971.

Sung JH, Mastri AR, Park SH. Axonal dystrophy in the gracile nucleus in children and young adults. J Neuropathol Exp Neurol 1981; 40: 37–45.

Takahashi T, Yagishita S, Amano N, Yamaoka K, Kamei T. Amyotrophic lateral sclerosis with numerous axonal spheroids in the corticospinal tract and massive degeneration of the cortex. Acta Neuropathol (Berl) 1997; 94: 294–9.

Trapp BD, Peterson J, Ransohoff RM, Rudick R, Mork S, Bo L. Axonal transection in the lesions of multiple sclerosis. N Engl J Med 1998; 338: 278–85.

Tu PH, Raju P, Robinson KA, Gurney ME, Trojanowski JQ, Lee VM. Transgenic mice carrying a human mutant superoxide dismutase transgene develop neuronal cytoskeletal pathology resembling human amyotrophic lateral sclerosis lesions. Proc Natl Acad Sci USA 1996; 93: 3155–60.

van Leeuwen FW, de Kleijn DP, van den Hurk HH, Neubauer A, Sonnemans MA, Sluijs JA, et al. Frameshift mutants of beta amyloid precursor protein and ubiquitin-B in Alzheimer's and Down patients. Science 1998; 279: 242–7.

Wang MS, Davis AA, Culver DG, Glass JD. Wld^S mice are resistant to paclitaxel (Taxol) neuropathy. Ann Neurol 2002; 52: 442–7.

Wilson SM, Bhattacharyya B, Rachel RA, Coppola V, Tessarollo L, Householder DB, et al. Synaptic defects in ataxia mice result from a mutation in Usp14, encoding a ubiquitin-specific protease. Nat Genet 2002; 32: 420–5.

Wujek JR, Lasek RJ. Correlation of axonal regeneration and slow component B in two branches of a single axon. J Neurosci 1983; 3: 243–51.

Yamazaki K, Wakasugi N, Tomita T, Kikuchi T, Mukoyama M, Ando K. Gracile axonal dystrophy (gad), a new neurological mutant in the mouse. Proc Soc Exp Biol Med 1988; 187: 209–15.

Zhai Q, Wang J, Kim A, Liu Q, Watts R, Hoopfer E, et al. Involvement of the ubiquitin–proteasome system in the early stages of Wallerian degeneration. Neuron 2003; 39: 217–25.

Cellular/Molecular

A Truncated Tropo-Myosine-Related Kinase B Receptor, T1, Regulates Glial Cell Morphology via Rho GDP Dissociation Inhibitor 1

Koji Ohira,[1,2] Haruko Kumanogoh,[1] Yoshinori Sahara,[1] Koichi J. Homma,[3] Hirohisa Hirai,[2] Shun Nakamura,[1] and Motoharu Hayashi[2]

[1]Department of Biochemistry and Cellular Biology, National Institute of Neuroscience, National Center of Neurology and Psychiatry, Tokyo 187-8502, Japan, [2]Department of Cellular and Molecular Biology, Primate Research Institute, Kyoto University, Inuyama, Aichi 484-8506, Japan, and [3]Department of Molecular Pathology, Faculty of Pharmaceutical Sciences, Teikyo University, Kanagawa 199-0195, Japan

Through tropo-myosine-related kinase B (TrkB) receptors, brain-derived neurotrophic factor (BDNF) performs many biological functions such as neural survival, differentiation, and plasticity. T1, an isoform of TrkB receptors that lacks a tyrosine kinase, predominates in the adult mammalian CNS, yet its role remains controversial. In this study, to examine whether T1 transduces a signal and to determine its function, we first performed an affinity purification of T1-binding protein with the T1-specific C-terminal peptide and identified Rho GDP dissociation inhibitor 1 (GDI1), a GDP dissociation inhibitor of Rho small G-proteins, as a signaling protein directly associated with T1. The binding of BDNF to T1 caused Rho GDI1 to dissociate from the C-terminal tail of T1. Astrocytes cultured for 30 d expressed only endogenous T1 among the BDNF receptors. In 30 d cultured astrocytes, Rho GDI1, when dissociated in a BDNF-dependent manner, controlled the activities of the Rho GTPases, which resulted in rapid changes in astrocytic morphology. Furthermore, using 2 d cultured astrocytes that were transfected with T1, a T1 deletion mutant, or cyan fluorescent protein fusion protein of the T1-specific C-terminal sequence, we demonstrated that T1-Rho GDI1 signaling was indispensable for regulating the activities of Rho GTPases and for the subsequent morphological changes among astrocytes. Therefore, these findings indicate that the T1 signaling cascade can alter astrocytic morphology via regulation of Rho GTPase activity.

Key words: astrocyte; BDNF; primary culture; Rho GDI; Rho GTPase; truncated TrkB; T1

Introduction

Brain-derived neurotrophic factor (BDNF) is enriched in the CNS and plays pivotal roles in neural survival, differentiation, and plasticity (Bibel and Barde, 2000; Thoenen, 2000). The effects of BDNF are transduced through the tropo-myosine-related kinase B (TrkB) receptor (Barbacid, 1994). There are three TrkB receptor isoforms in the mammalian CNS (Barbacid, 1994). The full-length isoform (TK+) is a typical tyrosine kinase receptor and transduces the BDNF signal (Kaplan and Miller, 2000). In contrast, two truncated isoforms (TK−: T1 and T2) possess the same extracellular domain, transmembrane domain, and first 12 intracellular amino acid sequences as TK+. However, the C-terminal sequences are the isoform specific (11 and 9 amino acids, respectively) (Barbacid, 1994).

Currently, TK−, especially T1, is hypothesized to be a dominant-negative form of TK+ and is involved in negative functions against TK+, such as the TK+ phosphorylation (Knüsel et al., 1994), the calcium efflux (Eide et al., 1996), the cell survival activity (Haapasalo et al., 2001), and gene expression by BDNF (Offenhäuser et al., 2002). According to this hypothesis, TK− is postulated to form the homodimer or heterodimer with TK+, which prohibits TK+ signaling or limits the availability of BDNF to the neural tissue by trapping excess BDNF.

In contrast, there are several findings that provide evidence against the hypothesis that T1 is a dominant-negative form of TK+. For example, the expression of T1 increases markedly at various important periods in the developing mammalian CNS, such as axonal remodeling and synaptogenesis (Allendoerfer et al., 1994; Fryer et al., 1996; Ohira et al., 1999, 2001). The specific alignment of the intracellular domain of T1 is completely identical among mice, rats, and humans (Klein et al., 1990; Middlemas et al., 1991; Shelton et al., 1995), suggesting that the alignment plays a unique role. In addition, T1 is capable of binding BDNF at the same level as does TK+ (Biffo et al., 1995). As regards the physiological function of T1, it is involved in the control of the elongation of distal dendrites of cortical pyramidal neurons (Ya-

Received May 26, 2004; revised Dec. 20, 2004; accepted Dec. 22, 2004.

This work was supported by Grants-in-Aid for Scientific Research on Priority Areas and the Advanced Brain Science Project (15016056 and 16015341 to M.H. and S.N.); by a Grant-in Aid for the Biodiversity Research of 21st Century Center of Excellence (A14) from the Ministry of Education, Culture, Sports, Science and Technology of Japan; and by Health Sciences Research grants from the Organization of Pharmaceutical Safety and Research and Research on Advanced Medical Technology (nano-1 and MF-3). We thank Dr. Hans Thoenen for his critical reading of this manuscript; Drs. Yoshihiro Sokawa, Shohei Maekawa, Takayoshi Inoue, and Nobuo Funatsu for their helpful comments; and Tomomi Ochiai-Ohira for her photographic expertise.

Correspondence should be addressed to Dr. Motoharu Hayashi, Department of Cellular and Molecular Biology, Primate Research Institute, Kyoto University, Kanrin, Inuyama, Aichi 484-8506, Japan. E-mail: hayashi@pri.kyoto-u.ac.jp.

DOI:10.1523/JNEUROSCI.4436-04.2005

 0270-6474/05/251343-11$15.00/0

coubian and Lo, 2000) and the BDNF-induced calcium entry in astrocytes (Rose et al., 2003). Based on these results, we considered a new hypothesis, namely, that T1 binds to proteins through its C-terminal-specific sequence, which elicits a unique type of signal transduction other than the well understood regulation of the tyrosine kinase pathway. In fact, T1 has been reported to mediate signal transduction (i.e., the acid metabolite release from cells) (Baxter et al., 1997).

To clarify the T1 signaling cascade, in this study, we first performed affinity purification with a T1-specific sequence and then identified Rho GDP dissociation inhibitor 1 (GDI1) as a T1 binding protein from the rat brain. Rho GDI1 is an inhibitory regulator of Rho GTPases that can regulate cell morphology via the remodeling of the cytoskeleton. Furthermore, we provide evidence that T1 is capable of ligand-mediated signaling through Rho GDI1 and of regulating astrocytic morphology in primary cultures.

Materials and Methods

Affinity chromatography. All experimental procedures for animals were performed in accordance with our institutional guidelines (1996). Young adult (4-week-old) Wistar rat whole brains (10 g) were homogenized in 10 vol of homogenization buffer (0.32 M sucrose, 5 mM Tris-HCl, pH 7.5, and 150 mM NaCl containing 1 mM PMSF, 10 μg/ml leupeptine, and 20 μg/ml aprotinin). After centrifugation at 100,000 × *g* at 4°C for 1 h, the supernatant was adjusted to a concentration of 1 mg/ml protein, and this solution was defined as the cytosolic fraction. Eleven synthesized amino acid residues (FVLFHKIPLDG) of the C terminal of T1 were conjugated to a poly-β-hydroxybutyrate-Tenta Gel S (Shimadzu, Kyoto, Japan) matrix. The affinity column was equilibrated with the homogenization buffer. Another column, without the synthetic peptides, was prepared as a control column. Ten milliliter aliquots of the cytosolic fraction were applied to the control column and then were loaded onto the affinity column. After the affinity column was washed with homogenization buffer containing 500 mM NaCl, the bound proteins were eluted in one step with 50 mM glycine, pH 2.5. Ten microliters of each fraction (200 μl) were subjected to SDS-PAGE (10% gel). The proteins in the gels were then silver stained.

Amino acid sequence analysis. The fractions containing the 28 kDa protein, which had been obtained from 20 independent affinity chromatography experiments, were concentrated using Centricon YM-10 (Millipore, Bedford, MA). The proteins were transferred to a polyvinylidene difluoride (PVDF) membrane (Millipore) using a buffer containing 10 mM 3-[(3-cholamidopropyl)dimethylammonio]-1-propanesulfonate and 10% methanol, pH 11. The membranes were stained with 0.1% Ponceau S in 1% acetic acid and were destained with distilled water. For the peptide sequence, immobilized protein bands were cut with 2 mg of CNBr and placed in 200 μl of 70% formic acid in an Eppendorf (Eppendorf Scientific, Westbury, NY) tube overnight. The resulting solution and membranes were dried and then boiled in SDS sample buffer. Tricine-SDS-PAGE was used to segregate the small peptides (<10 kDa) (Ploug et al., 1989). The cut peptides were transferred to PVDF^{SQ} membranes (Millipore), which were then stained with 0.1% Ponceau S in 1% acetic acid and destained with distilled water. The bands were applied to a Sequencer (476A protein sequencer; Applied Biosystems, Foster City, CA).

Cell cultures. For the cell cultures, human embryonic kidney 293 (HEK293) cells were kept in DMEM supplemented with 10% FBS. Astrocytic primary cultures were prepared from neonatal rat pups (Sprague Dawley). The hippocampi were cut into 1 mm slices, incubated in activated papain (20 U/ml, 20 min), and dissociated by gentle trituration (Sahara and Westbrook, 1993). Dissociated astrocytes from neonatal rats were plated at 300,000 cells per dish on cover glasses coated with poly-L-lysine (Sigma, St. Louis, MO). The culture medium contained MEM (Invitrogen, Carlsbad, CA), 0.6% glucose, 5% heat-inactivated FBS, and penicillin–streptomycin (Invitrogen). At 3 d *in vitro* (DIV) after plating, the expression plasmid vectors (see below) were transfected into astrocytes with Lipofectamine 2000 (Invitrogen). At 4 h after transfection, the culture media were exchanged to DMEM containing N2 supplement (Invitrogen). After 24 h, the cells were used for the experiments. For the long-term cultured astrocytes, cells were incubated in DMEM with 5% FBS, and the medium was exchanged every 3 d. At 72 h before the experiments, the culture media were replaced with DMEM containing the N2 supplement. Additionally, the media of all cultures were exchanged for fresh media at 2 h before the experiments.

Reverse-transcription PCR. Total RNA was isolated from primary astrocytes with Isogen (Nippon Gene, Tokyo, Japan). Total RNA (2 μg) was reverse transcribed into cDNA in 20 μl of 1× first-strand buffer containing 0.5 μg of oligo-dT as a primer, 500 μM dNTP, and 200 U of SuperScript II (Invitrogen). PCR was performed in 20 μl of 1× PCR buffer containing 2 μl of reverse transcription (RT) products, 1 U of AmpliTaq DNA polymerase (Roche Applied Science, Basel, Switzerland), 200 μM dNTP, and 0.4 μM of the primer pair. We used the endogenous internal standard (β-actin, 5′-TAAAACGCAGCTCAGTAACAGTCCG-3′ and 5′-TGGAATCCTGTGGCATCCATGAAAC-3′; 348 bp) and specific primers for TK+ (5′-ATAACGGAGACTACACCCTGATGG-3′ and 5′-AGCTGACTGTTGGTGATGCC-3′; 505 bp), T1 (5′-CATAAGATCCCACTGGATGGGTAG-3′ and 5′-GCTGCAGACATCCTCGGAGATTAC-3′; 177 bp), T2 (5′-CAGAAGTGTGCTTATTTTGC-3′ and 5′-AGACAATACAGGTCTACCTCTCAG-3′; 553 bp), or p75 (5′-TGTGTGAAGAGTGCCCAGAG-3′ and 5′-TCACCATATCCGCCACTGTA-3′; 263 bp). The PCR parameters were 94°C for 30 s, 58°C for 30 s, and 72°C for 60 s for 30 cycles, followed by a final elongation at 72°C for 5 min. The amplified PCR products were separated on 1.5% agarose gel.

DNA constructs and transfection. The T1 cDNA obtained from the adult rat cortex was subcloned into the *Eco*RI sites of p internal ribosomal entry site (IRES) 2-enhanced green fluorescent protein (EGFP) (Clontech, Palo Alto, CA), and the resulting construct was designated as pT1-IRES-EGFP. Mutant constructs of T1 were prepared by a PCR mutagenesis method. Briefly, we used the 5′ primer for T1, GGTCTGCCGTCTGCACGTCTG, and the 3′ primers A, CGCGGATCCCTAGAGCAGAAGCAGCATC; B, CGCGGATCCTTAACCTTTCATGCC; C, CGCGGATCCCTAAACAAAACCTTTC; D, CGCGGATCCCTAATGAAACAAAACAAAAC; and E, CGCGGATCCCTAGGGGATCTTATG. The underlined sequences indicate the *Bam*H1 sites. The boldface letters represent mutation sites. PCR was performed at 94°C for 30 s, 58°C for 30 s, and 72°C for 60 s for 30 cycles, followed by a final elongation at 72°C for 5 min with an Expand High Fidelity PCR system (Roche Applied Science). The amplified PCR products were separated on 2% agarose gel. The PCR products were digested at the 5′ *Bst*PI and the 3′ *Bam*H1 sites, and the digested products were subcloned into pT1-IRES-EGFP. The vectors of enhanced cyan fluorescent protein (ECFP)-Δ11 and ECFP-intracellular domain (ICD) were also prepared by PCR, using the 5′ primer GGTCTGCCGTCTGCACGTCTG and the 3′ primer of Δ11, CGCGGATCCTTAACCTTTCATGCC or the 3′ primer of ICD, CGCGGATCCCCCAGCCTTGTCTTTCCTTTATC. The deletion mutants are shown in Figure 3. The underlined sequences indicate the *Bam*H1 sites, and the boldface letters represent mutation sites. PCR was performed at 94°C for 30 s, 58°C for 30 s, and 72°C for 60 s for 30 cycles, followed by a final elongation at 72°C for 5 min with an Expand High Fidelity PCR system (Roche Applied Science). The amplified PCR products were separated on 2% agarose gel. The PCR products were digested by the 5′ and 3′ *Bam*H1 sites and were then subcloned into these sites of pECFP-C1 (Clontech). These constructs were transfected into HEK293 cells and astrocytes with Lipofectamine 2000.

Production of glutathione S-transferase-fusion proteins and in vitro binding assay. Constructs of glutathione *S*-transferase (GST)-fusion proteins were prepared by a PCR method. For the preparation of GST-T1-ICD, we used the above pT1-IRES-EGFP as a template, the 5′ primer CAAGAATTCCTCCAAGTTGGCGAGACATTCC, and the 3′ primer GTTGTCGACTTGTCTTTCCTTTATCTCAG. The single-underlined sequence indicates the *Eco*RI site, and the double-underlined sequence indicates the *Sal*I site. PCR was performed at 94°C for 30 s, 58°C for 30 s, and 72°C for 60 s for 25 cycles, followed by a final elongation at 72°C for 5 min with an Expand High Fidelity PCR system. The digested PCR product was subcloned into the pGEX-5X-3 bacterial expression vector

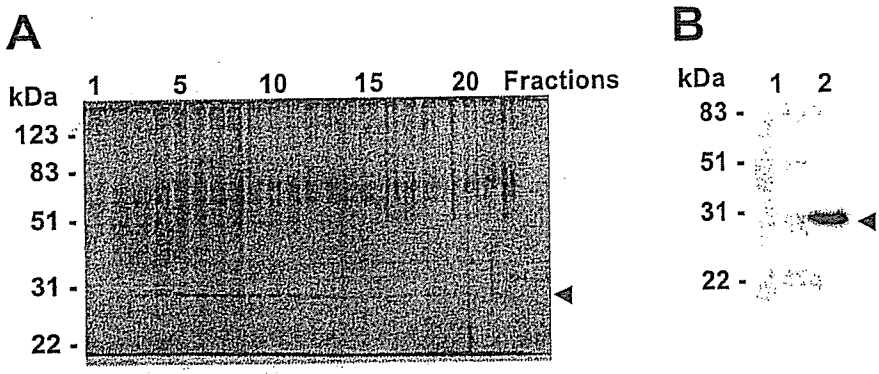

Figure 1. Affinity purification of a binding protein of T1. *A*, The cytosolic fraction from rat brain was loaded onto an affinity column with the T1 synthetic peptide. One-step elution with glycine (50 mM; pH 2.5) was performed, and elution samples from the column were separated; an aliquot of each eluate was subjected to SDS-PAGE (10% gel). The resulting silver-stained gel image is shown here. The arrowhead indicates the position of the 28 kDa protein. *B*, Western blot analysis of the eluate from the control column (lane 1) and the affinity column (lane 2) with anti-Rho GDI1. The arrowhead indicates the position of Rho GDI1 (28 kDa).

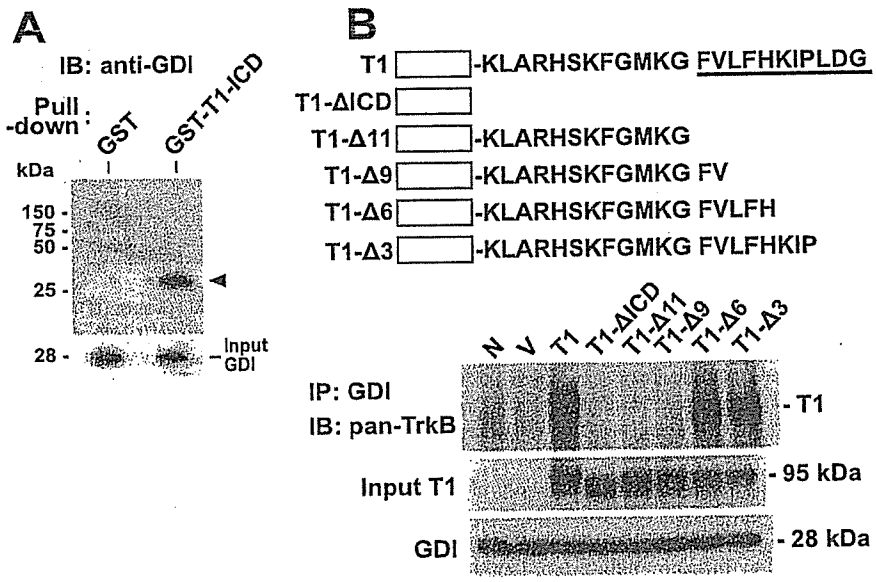

Figure 2. Direct binding of Rho GDI1 to T1 and binding motif in the T1-specific sequence. *A*, The GST moiety or the GST-T1-ICD was mixed with recombinant Rho GDI1 in Eppendorf tubes. The GST proteins were precipitated with glutathione-Sepharose 4B. The coprecipitated Rho GDI1 was detected with anti-Rho GDI1. The arrowhead indicates Rho GDI1 (28 kDa). *B*, The Rho GDI1 binding site in the intracellular domain of T1. A display of T1 and its deletion mutants is shown in the top panel. The white boxes represent the extracellular and transmembrane domains, and the underlined sequence indicates the specific amino acid sequence of T1. The constructs were transfected into HEK293 cells. After 24 h, coimmunoprecipitation with anti-Rho GDI1 was performed. N, No vector; V, empty vector expressing GFP; T1, normal T1; T1-ΔICD, T1 without its ICD; T1-Δn, T1 deletion mutants lacking the indicated number of amino acids from the C terminal. IB, Immunoblot; IP, immunoprecipitation.

(Amersham Biosciences, Piscataway, NJ). To obtain the cDNA of Rho GDI1, we used a cDNA library of the adult mouse cortex as a template, the 5′ primer CACGAATTCTAGGGCAGAACAGGACC, and the 3′ primer GTTGTCGACTAGGTAGGGGGTTAG. A single-underlined sequence indicates the *Eco*RI site, and a double-underlined sequence indicates the *Sal*I site. The boldface letter in the 5′ primer of GST-Rho GDI1 is the point mutation site. The methods used for PCR preparation and subcloning into the pGEX-5X-3 vector were the same as those used for T1. After the OD_{600} reached 0.6, 1 mM isopropyl-1-thio-β-D-galactopyranoside was added to the cultures, and *Escherichia coli* were grown for an additional 16 h at 25°C (Yamashita and Tohyama, 2003). After the cells were collected, they were resuspended in PBS and sonicated. To the cell lysates, 0.5% Triton X-100 was added, and the samples were incubated for 30 min at 4°C. After centrifugation at 10,000 × *g* for 5 min, glutathione-Sepharose 4B (Pharmacia, Piscataway, NJ) was added to the supernatants, which were then incubated for 30 min at 4°C. After centrifugation at 10,000 × *g* for 5 s, the beads were washed three times in PBS containing 0.5% Triton X-100. The purity of the proteins was determined by SDS-PAGE. Then, glutathione-Sepharose 4B with GST-T1-ICD was used for the binding assay. To remove the GST moiety from GST-Rho GDI1, Factor Xa (Novagen, Darmstadt, Germany) was added to the glutathione-Sepharose 4B with GST-Rho GDI1, and the samples were incubated for 16 h at 20°C. After centrifugation at 10,000 × *g* for 5 min, Xarrest agarose (Novagen) was added to the supernatants, and the samples were incubated for 10 min at room temperature. After centrifugation at 1000 × *g* for 5 min, the supernatants were designated as the recombinant Rho GDI1 without GST. To check the cleavage of GST-Rho GDI1, glutathione-Sepharose 4B was added into the supernatant of Rho GDI1, and the samples were incubated for 30 min at 4°C. After centrifugation at 10,000 × *g* for 5 min, the precipitates were washed three times in PBS containing 0.5% Triton X-100, and they were then boiled in SDS sample buffer (see supplemental Fig. 1, available at www.jneurosci.org as supplemental material).

For the *in vitro* binding assay, recombinant Rho GDI1 solution was added to the glutathione-Sepharose 4B with GST-T1-ICD, and the samples were incubated for 1 h at 4°C with agitation. After centrifugation at 10,000 × *g* for 5 s, the precipitates were washed three times in PBS containing 0.5% Triton X-100, and then they were boiled in SDS sample buffer.

Precipitation assays. After each incubation with reagents, the cells were lysed with 0.15 ml of lysis buffer. For Rho GDI1-T1 coimmunoprecipitation, lysis buffer A (10 mM triethanolamine, 10 mM iodoacetoamine, pH 7.8, 150 mM NaCl, 2 mM EDTA, 1% digitonin, 1 mM PMSF, 10 μg/ml leupeptin, and 20 μg/ml aprotinin) was used. The lysates were centrifuged at 10,000 × *g* at 4°C for 20 min. Then, 50 μl aliquots of resulting supernatants were designated as total protein samples. Normal mouse IgG and protein G-Sepharose were added to the remaining supernatants, which were incubated at 4°C for 1 h with gentle rotation. After centrifugation at 5000 × *g* at 4°C for 1 min, mouse monoclonal anti-pan-TrkB (2 μl; Transduction Laboratories, Lexington, KY) or rabbit polyclonal anti-Rho GDI1 (3 μl; Santa Cruz Biotechnology, Santa Cruz, CA) was added. In the competitive assays with the synthetic peptides of the T1 C terminal, the peptides (final concentration, 100 μM and 1 mM) were added to the lysates and incubated at 4°C for 1 h. The samples were incubated at 4°C for 2 h with antibody and then were incubated with protein G-Sepharose at 4°C for 1 h with gentle rotation. The precipitates were washed four times with lysis buffer A and boiled in 40 μl of SDS sample buffer for 3 min.

For the RhoA, Rac1, and Cdc42 pull-down assay, we used lysis buffer B [50 mM Tris-HCl, pH 7.5, 150 mM NaCl, 5 mM $MgCl_2$, 0.5% Triton X-100, 1 mM PMSF, 10 μg/ml leupeptin, 20 μg/ml aprotinin, and 10 nM microcystin LR (Leu and Avg)]. The lysates were centrifuged at 10,000 × *g* at 4°C for 20 min. We then performed the RhoA pull-down assay with Rhotekin beads (Upstate Biotech, Charlottesville, VA) according to the method of Ren et al. (1999) and the Rac1 and Cdc42 pull-down assay with p21-activated kinase (PAK) beads (Upstate Biotech). Then, the Rhotekin (Upstate Biotech) or PAK beads (30 μl) were added to the lysates (1 mg of protein/ml) and incubated at 4°C for 45 min. The beads

were washed three times with lysis buffer B. The pellets were then mixed with 40 μl of SDS sample buffer and boiled for 3 min. In the control assays using GTPγS- and GDP-loaded lysates, we confirmed our assay systems (supplemental Fig. 2, available at www.jneurosci.org as supplemental material). Briefly, 3 μl of 0.5M EDTA (10 mM) and then 1.5 μl of GTPγS (100 μM) or GDP (1 mM) was added to a 0.15 ml aliquot of each cell extract. The extracts were incubated at 30°C for 30 min. To stop the loading of GTPγS and GDP, we added 9 μl of 1 M $MgCl_2$ (60 mM). The procedures that were subsequently performed have been described above.

Western blot analysis. Using an aliquot of astrocytic culture lysates, we also performed a Western blot analysis of protein expression. The samples (5 μg total protein per lane, except for TrkB, Cdc42, and Rac1, as follows: 100 μg total protein per lane for TrkB, Cdc42, and Rac1 and 10 μl per lane for the precipitates) were subjected to SDS-PAGE and then were blotted onto PVDF membranes. The membranes were blocked for 1 h in 5% skim milk in PBS [containing (in mM): 137 NaCl, 8.1 $Na_2HPO_4 \cdot 7H_2O$, 2.7 KCl, and 1.5 KH_2PO_4]. After incubation with the primary antibodies at room temperature for 1 h, the blots were incubated for 1 h with secondary antibodies conjugated with HRP and then were visualized by the ECL system (Amersham Biosciences). For the primary antibodies, we used anti-pan-TrkB (1:200; Santa Cruz Biotechnology), anti-TK+ (1:200; Santa Cruz Biotechnology), anti-T1 (1:200; Santa Cruz Biotechnology), anti-RhoA (1:200; Santa Cruz Biotechnology), anti-Rac1 (1:1000; Transduction Laboratories), anti-Cdc42 (1:1000; Transduction Laboratories), anti-Rho GDI1 (1:200; Santa Cruz Biotechnology), and anti-β-tubulin (1:1000; Sigma).

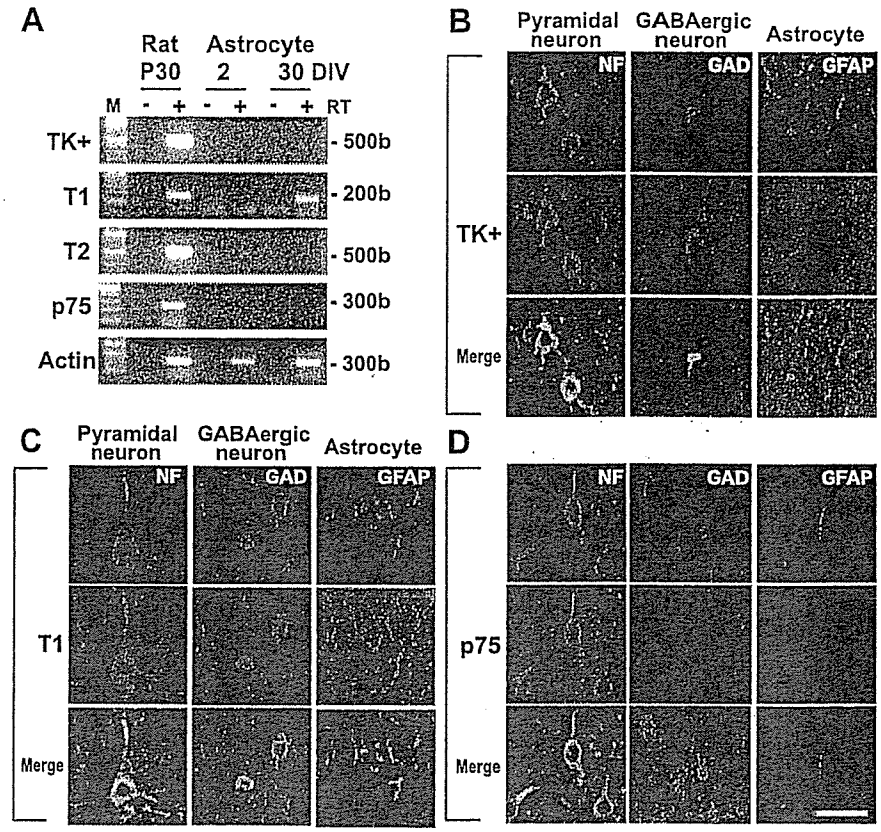

Figure 3. Expression of BDNF receptors in astrocytes in primary culture and young adult rat brain. *A*, RT-PCR analysis of TrkB subtypes and p75 expression in P30 rat neocortex and astrocytes at 2 and 30 DIV. M, 100 base marker. *B–D*, Distributions of TK+, T1, and p75 in the young adult (4-week-old) rat cortex. Astrocytes in layers I/II, pyramidal neurons, and GABAergic neurons in layers V/VI of the motor cortex are represented. Pyramidal neurons, GABAergic neurons, and astrocytes immunostained using anti-neurofilament (NF), anti-GAD (GAD), and anti-GFAP (GFAP), respectively, are shown in red. The immunopositive structures of TK+, T1, and p75 are shown in green. The double-positive cells in the merged images are shown in yellow-green. Scale bar, 20 μm.

Immunohistochemistry. Young adult rats (4-week-old Wistar rats) were anesthetized and perfused with 4% formaldehyde in phosphate buffer. The brains were postfixed for 6 h and cryoprotected in 30% sucrose in PBS. The brains were mounted in Tissue-Tek (Miles, Elkhart, IN), frozen rapidly on dry ice, and stored at −30°C. The sections were cut to a thickness of 35 μm with a cryostat (Leica, Wetzlar, Germany). The sections were mounted on glass slides coated with 3-aminopropyltriethoxysilane, washed for 30 min with PBS, and then preincubated with PBS-GB [4% normal goat serum (Vector Laboratories, Burlingame, CA) and 1% bovine serum albumin in PBS] for 2 h at room temperature. The sections were incubated for 48 h at 4°C with antibodies. We used the following primary antibodies: rabbit polyclonal anti-TK+ (1:800) and anti-T1 (1:800) and mouse monoclonal anti-neurofilament (1:1000; clone SMI32; Sternberger Monoclonals, Lutherville, MD), anti-glutamic acid decarboxylase (GAD; 1:3000; Affinity Research Products, Exeter, UK), and anti-glial fibrillary acidic protein (GFAP; 1:1000; Chemicon, Temecula, CA). The sections were incubated for 1 h at room temperature with the following secondary antibodies: anti-mouse IgG cyanine 3 (Cy3; 1:200; Chemicon) and anti-rabbit IgG Alexa 488 (1:200; Molecular Probes, Eugene, OR). The sections were embedded with Permafluor (Thermo Shandon, Pittsburgh, PA). We used a confocal microscope (TCS SP2; Leica) to analyze the samples.

Morphological assays. The cells were stimulated for the indicated periods at 37°C with 20 ng/ml BDNF (PeproTech, Rocky Hill, NJ) or 100 ng/ml NGF (PeproTech) or vehicle. The cell samples were also incubated for 20 min with anti-BDNF (5 μg/ml; Santa Cruz Biotechnology) and then were incubated for 30 min with 20 ng/ml BDNF. For treatment with Toxin A (Biogenesis, Poole, UK) and C3 toxin (Calbiochem, La Jolla, CA), we performed the procedures according to methods described previously (Just et al., 1995; Maekawa et al., 1999). Toxins (20 ng/ml of Toxin A, 30 μg/ml of C3 toxin) were added to the 30 DIV cells, and the cells were incubated for 24 h at 37°C. The cells were washed twice in PBS and then were fixed in 4% formaldehyde in PBS for 1 h at room temperature. The cells were preincubated with PBS-GB and were incubated with anti-GFAP for 48 h at 4°C. After being washed in PBS, the cells were incubated with anti-mouse IgG Cy3. The cells were then embedded with Permafluor. We used a confocal microscope for the analysis. For the time-lapse analysis, the astrocytic cultures were set on the confocal microscope (TCS SP2; Leica) with oxygen supply. Phase-contrast images were taken using a 40× water-immersion objective at indicated time. Each cell area was measured by AquaCosmos (Hamamatsu Photonics K.K., Hamamatsu, Japan).

Results

Rho GDI1 is a T1-binding protein

T1 exhibits a characteristic developmental expression pattern in the mammalian CNS (i.e., the expression of T1 is known to be remarkably increased after birth and is a major product among TrkB subtypes in adults) (Allendoerfer et al., 1994; Fryer et al., 1996; Ohira et al., 1999). Thus, we purified T1-binding proteins from the cytosolic fraction of adult rat brains, using an affinity column conjugated with the C-terminal-specific sequence of T1. A 28 kDa protein was eluted from the column as a sharp peak under low pH conditions using glycine buffer, pH 2.5 (Fig. 1*A*). The fractions containing the protein eluted from the affinity column were concentrated by a centrifugal concentrator. Then, the 28 kDa protein was purified as a single band blotted on a PVDF membrane and cleaved by CNBr. The resulting peptides were

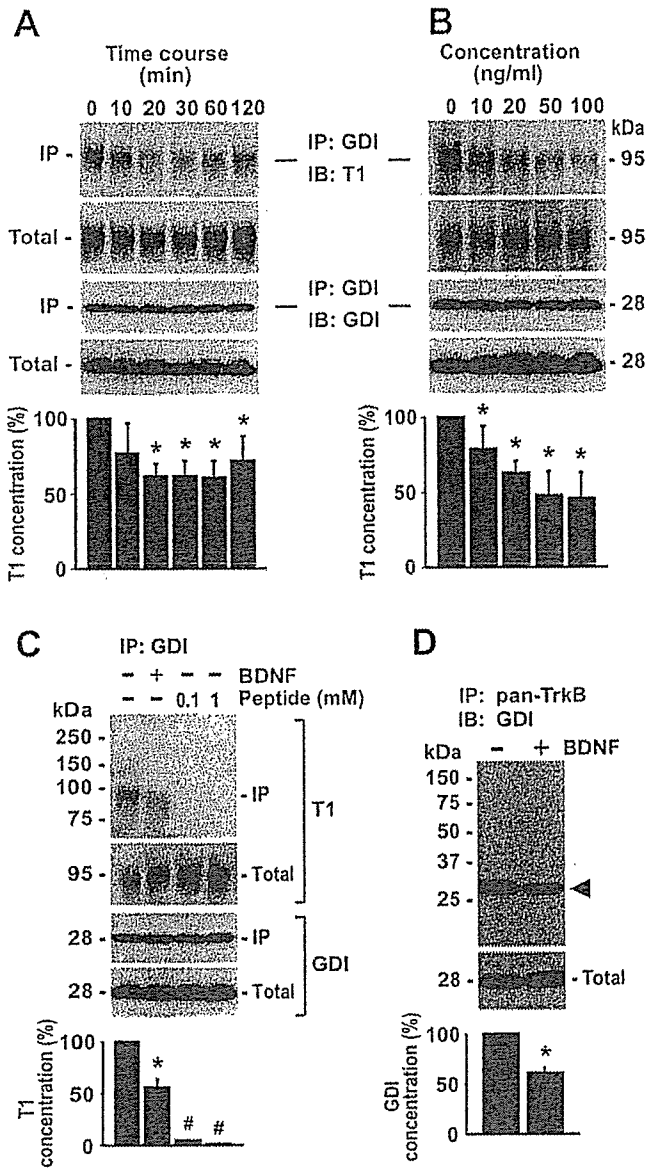

Figure 4. Dissociation of Rho GDI1 from T1 by BDNF treatment in 30 DIV astrocytes. *A*, Coimmunoprecipitation of T1 with anti-Rho GDI1 at each time point after BDNF stimulation (20 ng/ml). *B*, Ligand-concentration dependency of the interaction between T1 and Rho GDI1 at 30 min after each concentration of BDNF stimulation. *C*, Competitive assay using the T1-specific peptides. The synthetic peptides of the T1 C terminal were added to the lysates of 30 DIV astrocytes. At the concentration of 100 μM and 1 mM, the T1 bands were hardly observed (lanes 3 and 4). *D*, Coimmunoprecipitation of Rho GDI1 with anti-pan-TrkB. Astrocytes were stimulated for 30 min by BDNF (20 ng/ml). The arrowhead indicates Rho GDI1 (28 kDa). Quantitative analysis of the bands in *A–D*. The control levels were taken as 100%. The asterisks indicate statistically significant differences ($p < 0.05$; one-way ANOVA and Scheffé's *post hoc* test). In *C*, the # symbol indicates significant differences between the BDNF and the peptide treatments ($p < 0.05$; one-way ANOVA and Scheffé's *post hoc* test). Values are given as means ± SD of four independent experiments. IB, Immunoblot; IP, immunoprecipitation.

separated by gel electrophoresis and blotted on a PVDF membrane to purify each band. The N-terminal sequence of one peptide was determined as KYIQHT according to the Edman degradation method. Consequently, this sequence was found to match the inner sequence of Rho GDI1, a Rho guanine nucleotide dissociation inhibitor that can stabilize the inactive, GDP-bound form of Rho GTPase (Takai et al., 2001). Western blot analysis identified the 28 kDa protein as Rho GDI1 (Fig. 1*B*).

In vitro binding assay

To examine whether T1 directly binds to Rho GDI1, we performed an *in vitro* pull-down assay using recombinant proteins (i.e., the GST-T1-ICD and Rho GDI1). As shown in Figure 2*A*, the GST moiety did not bind to Rho GDI1, whereas the GST-T1-ICD fusion protein precipitated Rho GDI1. The possible contribution of the direct binding of GST-Rho GDI1 to glutathione-Sepharose 4B as a result of incomplete cleavage could be excluded, because we detected the Rho GDI1 at 28 kDa but not the 54 kDa band of the fusion protein. Therefore, we concluded that T1 directly binds to Rho GDI1.

Binding motif of T1 with Rho GDI1

We further determined a specific motif of T1 binding to Rho GDI1 using deletion mutants of the C terminal of T1. Constructs of T1 lacking its intracellular domain (T1-ΔICD) and T1 deletion mutants lacking the indicated number of amino acids from the C-terminal domain (T1-Δn) were transfected into HEK293 cells, and coimmunoprecipitation with anti-Rho GDI1 antibody was performed at 24 h after transfection. We detected the bands of both T1-Δ3 and T1-Δ6 at ~95 kDa, which was comparable with those of normal T1 (Fig. 2*B*). However, deletion mutants lacking nine or more amino acids were no longer able to bind to Rho GDI1. Thus, the present results suggested that LFH in the T1-specific sequence (FVLFHKIPLDG) is responsible for binding to Rho GDI1.

Expression of BDNF receptors in astrocytic primary cultures and adult rat brains

T1 has been reported to be distributed in both neurons and glia (Frisén et al., 1993; Armanini et al., 1995; Ohira and Hayashi, 2003). In astrocytic primary cultures from the neonatal rat hippocampus, RT-PCR analysis did not reveal the mRNA expression of any of the TrkB subtypes or of p75 at 2 DIV after plating (Fig. 3*A*). Astrocytes cultured long-term (30 DIV) expressed T1 mRNA, whereas no TK+, T2, or p75 mRNA expression was detected. We also examined the distribution of T1 in the adult rat cortex using fluorescent double-staining histochemistry. In this series, the following cell markers were used: neurofilament for pyramidal neurons, GAD for GABAergic neurons, and GFAP for astrocytes. TK+ immunoreactivity was localized in both pyramidal and GABAergic neurons but not in astrocytes (Fig. 3*B*). In contrast, T1 immunoreactivity was detected not only in both pyramidal and GABAergic neurons, but also in the astrocytes (Fig. 3*C*). The neurotrophin receptor p75 (p75) was only expressed in the pyramidal neurons (Fig. 3*D*). Together, these results indicate that astrocytes in the cortex and hippocampus of adult rats possess only T1 among the known BDNF receptors. Therefore, we used rat hippocampal astrocytes to investigate the signaling mechanism of T1.

Dissociation of Rho GDI1 from T1 in a BDNF-dependent manner

To determine whether Rho GDI1 dissociated from T1 in a BDNF-dependent manner in long-term cultured (30 DIV) astrocytes, we performed a pull-down assay of T1 with anti-Rho GDI1 antibody, and we detected T1 using anti-T1 antibody. As shown in Figure 4*A*, the T1 band was reduced to ~60% of the control level at 20 min after BDNF treatment (20 ng/ml). The reduced levels of T1 bands were maintained for 60 min, and then a less significant reduction in T1 bands (70% of the control level) was observed at 120 min after the addition of BDNF. Moreover, the dissociation of Rho GDI1 from T1 appeared to occur in a dose-

dependent manner (Fig. 4*B*). We found that 50 ng/ml BDNF stimulation for 30 min led to the adequate dissociation of Rho GDI1, which then reached a plateau level (50% of control level).

Furthermore, to determine whether the interaction between T1 and Rho GDI1 was specific, we performed the peptide competition assays using the T1-specific C-terminal peptide. The peptides were added to the lysates derived from 30 DIV astrocytes to a final concentration of 100 μM or 1 mM. Both additions of 100 μM and 1 mM peptides significantly inhibited the interaction (4.7 and 1.4% of control level, respectively) (Fig. 4*C*). Because Rho GDI1 was immunoprecipitated by anti-Rho GDI1 in the competitive assays (Fig. 4*C*, lanes 3 and 4), which was comparable with the control level (Fig. 4*C*, lane 1), the peptides specifically blocked the T1 binding to Rho GDI1.

In addition, we performed a pull-down assay of Rho GDI1 using anti-pan-TrkB antibody, and we detected Rho GDI1 using anti-Rho GDI1 antibody; this approach thus reversed the use of the antibodies to confirm the interaction between T1 and Rho GDI1. Then, we found that the Rho GDI1 band was reduced by 60% of the control level by BDNF treatment (Fig. 4*D*), which was comparable with the results of the pull-down assay performed with anti-Rho GDI1. Therefore, these findings suggest that treatment with BDNF can lead to the dissociation of Rho GDI1 from T1. In the subsequent experiments, to obtain sufficient dissociation of Rho GDI1 from T1, we applied 20 ng/ml BDNF for 30 min to astrocytic cultures. At the concentration of 20 ng/ml BDNF, p75 cannot function (Dechant and Barde, 1997), even through p75 expression remained below the levels that could be detected by PCR (Fig. 3*A*).

BDNF effects on astrocytic morphology in 30 DIV cultures

Rho GTPases are involved in the regulation of cell morphology by remodeling the cytoskeleton, which contains microfilaments, intermediate filaments, and microtubules (Ridley, 2001; Etienne-Manneville and Hall, 2002). Rho GDI1 has been shown to selectively interact with the GDP-bound forms of the Rho GTPases and to inhibit their conversion from the GDP-bound inactive form to the GTP-bound active form (Takai et al., 2001). Thus, we examined the morphological alteration of astrocytes by endogenous T1 in 30 DIV cultures. In serum-free medium containing N2 supplement, the form of 30

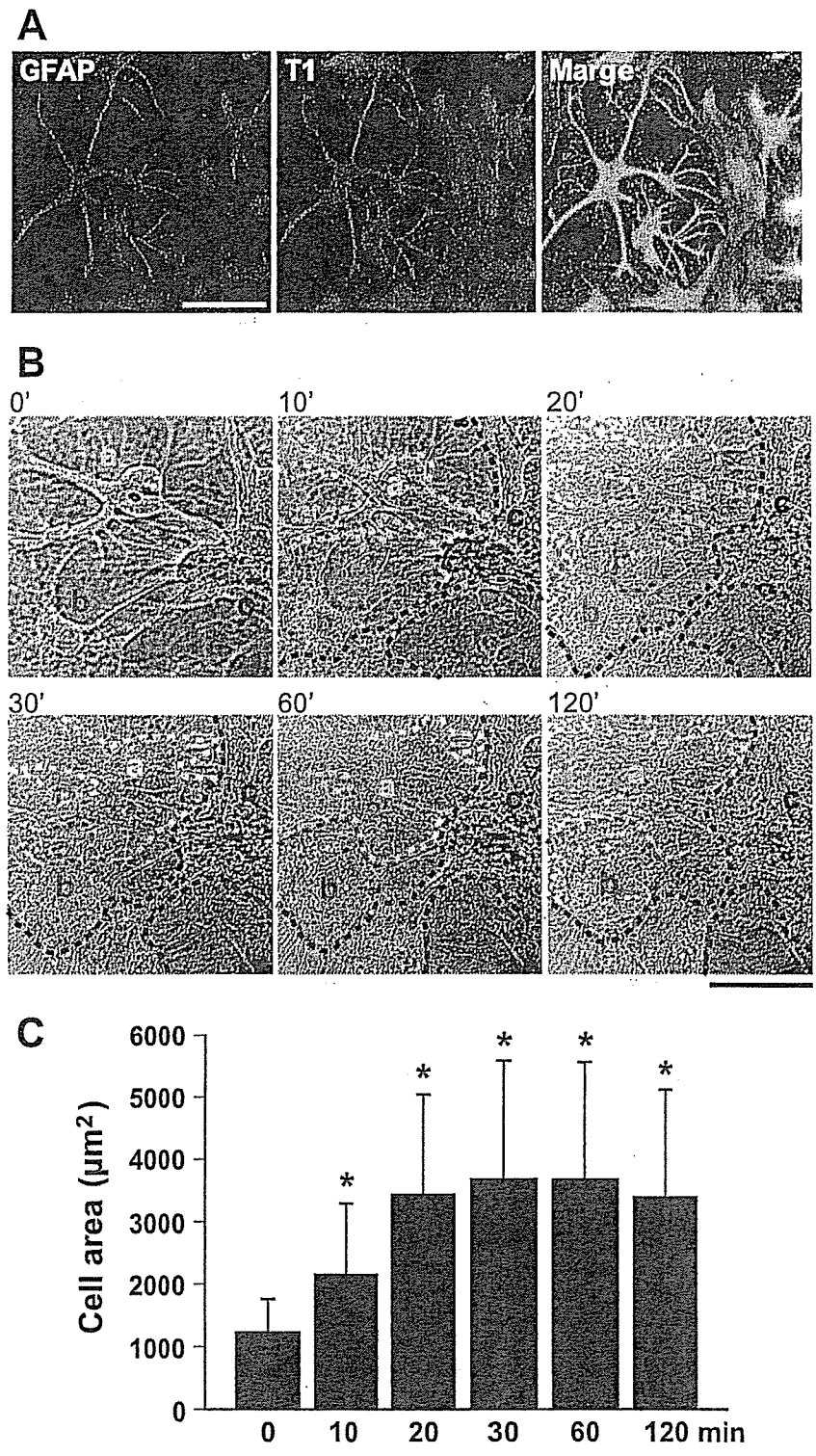

Figure 5. Morphological changes in astrocytes in 30 DIV astrocytic cultures. *A*, Coexpression of GFAP and T1 in the 30 DIV astrocytes. The cells were incubated in DMEM containing N2 supplement without BDNF stimulation and fixed in 4% formaldehyde. The immunoreactive cells for GFAP and T1 were stained by red and green, respectively. The cells coexpressing both GFAP and T1 were yellow. Note that almost all cells were coimmunopositive. Scale bar, 50 μm. *B*, Time-lapse images of the 30 DIV astrocytic cultures by the phase-contrast microscope. BDNF (20 ng/ml) was added to the 30 DIV cultures at 0 min. The number in each photograph indicates the time lapse (in minutes) after BDNF treatment. Three cells were marked by the colored small letter, yellow "a," red "b," and black "c," and they were also outlined by the dotted lines of corresponding colors. Note that the more the time passed, the thinner the cell bodies and processes were. Scale bar, 20 μm. *C*, Quantification of cell size. Values are given as the means ± SD of the cell size analysis based on the results of four independent experiments (total cell counts: 0 min, $n = 944$; 10 min, $n = 1003$; 20 min, $n = 978$; 30 min, $n = 981$; 60 min, $n = 1105$; 120 min, $n = 1054$). The asterisks indicate significant differences ($p < 0.05$; one-way ANOVA and Scheffé's *post hoc* test) compared with the value at 0 min.

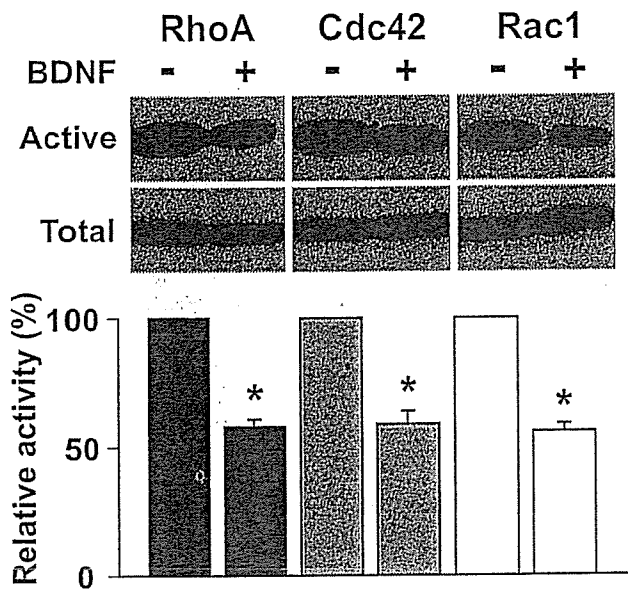

Figure 6. Activities of Rho GTPases in 30 DIV astrocytic cultures. Top, The cells were stimulated for 30 min with BDNF (20 ng/ml), and the cell extracts were subjected to *in vitro* binding assays. The precipitates and total proteins (5 μg for RhoA; 100 μg for Cdc42 and Rac1) were loaded on 15% gel and were detected with specific antibodies. Bottom, Quantitative analysis of the bands shown in the above images. Each control level, without BDNF stimulation, was taken as 100%. The asterisks indicate statistically significant differences ($p < 0.05$; paired Student's *t* test). Values are given as means ± SD of four independent experiments.

DIV astrocytes became fibrous (Fig. 5*A*,*B*). Almost all astrocytes were immunoreactive for both GFAP and T1 (Fig. 5*A*). The time-lapse analysis showed that BDNF stimulation led to a dynamic change in the shape of the astrocytes from fibrous to flat within 30 min (Fig. 5*B*). The cell surface area significantly increased 1.7-fold at 10 min and reached a threefold plateau level at 30 min (Fig. 5*C*). At 120 min after BDNF stimulation, the cells had decreased in size, albeit not significantly. At the same time, we measured the activities of RhoA, Rac1, and Cdc42, which are substrates of Rho GDI1, at 30 min when the change in astrocytic morphology reached a maximum. The active forms of all Rho GTPases were reduced by 60% of the control level (Fig. 6). The observed alterations in the shape of the astrocytes and the changes in Rho GTPase activity were both closely associated with the interaction between T1 and Rho GDI1 (Fig. 4), suggesting that BDNF-T1-Rho GDI1 signaling might control the Rho GTPases and consequently alter astrocytic morphology.

To elucidate the mechanism by which Rho GTPases regulate astrocytic morphology, we performed an inhibition assay of Rho GTPases using Toxin A and C3 toxin, which are known to inhibit all Rho GTPases (RhoA, Cdc42, and Rac1) and RhoA, respectively, in 30 DIV cultures. The astrocytic cultures were stimulated by BDNF at 20 ng/ml for 30 min. The results of the control cells were the same as the time-lapse analysis above (Fig. 7*A*). The astrocytes without BDNF treatment had long processes. Being treated by BDNF, the shapes of astrocytes were flat. In the Toxin A-treated cultures, the morphology of astrocytes was flat, regardless of BDNF treatment (Fig. 7*A*), which was similar to the shapes of the BDNF-treated control cells. The size of the cells was the same as that of BDNF-treated normal astrocytes (Fig. 7*B*). In contrast, C3 toxin treatment left the astrocytic morphology fibrous with fine filopodia-like processes (Fig. 7*A*). After BDNF treatment, the cells flattened; these findings were comparable with the observed morphology and size of the BDNF-treated control cells and the Toxin A-treated cells (Fig. 7*A*). Therefore, endogenous T1 might alter astrocytic morphology (i.e., it renders astrocytes fibrous and flat) via the control of Rho GTPases and primarily through Cdc42 and Rac.

Involvement of T1 in the regulation of astrocytic morphology

We examined the molecular mechanism of the T1-induced morphological alteration of astrocytes by performing a transfection assay with T1 mutants. Because 30 DIV astrocytes were refractory to transfection (<5%), whereas short-term cultured astrocytes (2 DIV) were easily transfected at high transfection efficiencies (>90%), we used 2 DIV astrocytes, in which we observed no expression of BDNF receptors (Fig. 3*A*).

First, we examined the effect of BDNF on the morphology of astrocytes overexpressing normal T1 or a T1 deletion mutant. Both the untransfected control cells and empty vector (GFP)-transfected cells showed a flat polygonal morphology with processes (Fig. 8). When these cells were treated with BDNF (20 ng/ml) for 30 min, we observed no changes in the cell morphology. On the other hand, the T1-transfected cells exhibited a fibrous, spindle morphology with long and narrow processes, even under the no-treatment condition. Interestingly, BDNF treatment rapidly and remarkably altered the cell morphology. Only 30 min after treatment with BDNF, the cells exhibited flat and wide cell bodies and stretched-out GFAP-positive fibers. The relative cell area of T1-transfected astrocytes treated with BDNF increased significantly, about fivefold, compared with that of T1-transfected astrocytes without BDNF treatment (Fig. 8*B*). In contrast, when T1-Δ11, a deletion mutant of a T1-specific sequence (Fig. 2*B*), was transfected, the cell morphology observed was a flat polygon with processes similar to those of the control, and BDNF treatment was not found to induce any morphological changes such as those found in the T1-transfected cells. Recently, p75 has been reported to associate with Rho GDI1 and regulate Rho activity (Yamashita et al., 1999; Yamashita and Tohyama, 2003). However, high-concentration treatment with NGF (100 ng/ml), which is a p75 ligand, had no effect on cell morphology. Taken together with the evidence that there was no morphological change in nontransfected cells or in GFP-expressing cells, it was concluded that p75 had no effect on cell morphology.

Next, we investigated whether BDNF negatively regulates the Rho GTPases through Rho GDI1 released from T1. To this end, we performed a pull-down assay of the active forms of the Rho GTPases. In astrocytes expressing exogenous T1, BDNF treatment was found to reduce the amount of activated RhoA, Cdc42, and Rac1 by 55, 51, 55% of the control level, respectively (Fig. 9). In contrast, cells expressing T1-Δ11 and cells treated with NGF (100 ng/ml) were not associated with a decrease in the active forms of RhoA, Cdc42, and Rac1. These results are compatible with findings regarding the regulation of Rho GTPase activity by endogenous T1 (Fig. 6). Thus, the present results suggest that the specific C-terminal alignment of T1 is necessary for the control of Rho GTPases and for the observed morphological alteration of astrocytes.

Competitive assay with T1 intracellular peptides

We then investigated the effects of the T1-specific C-terminal peptide on the regulation of astrocytic morphology. To inhibit the T1 signaling cascade in a competitive manner, we cotransfected the expression vectors of T1 and each of the following: CFP, CFP-Δ11, and CFP-ICD. We expected that CFP-ICD, but not CFP or CFP-Δ11, would trap Rho GDI1 within the cytoplasmic region and inhibit the association of Rho GDI1 to the Rho

GTPases, thereby resulting in the inhibition of the activity of BDNF. As shown in Figure 10, *A* and *B*, when both CFP and CFP-Δ11 were transfected with normal T1, we observed fibrous astrocytes under the condition lacking BDNF treatment. The addition of BDNF induced the morphological alteration of the astrocytes from fibrous to flat for 30 min. Namely, neither CFP nor CFP-Δ11 blocked the effects of BDNF, compared with the results obtained with the transfectant with T1-expression vector alone (Fig. 8). On the other hand, when CFP-ICD was overexpressed, the cells exhibited the same fibrous characteristics as were observed in the cases of the CFP- and CFP-Δ11-transfected cultures. However, BDNF treatment was not found to induce morphological changes among the astrocytes that remained fibrous. Therefore, the T1-specific sequence was determined to be indispensable for the morphological alteration of these astrocytes.

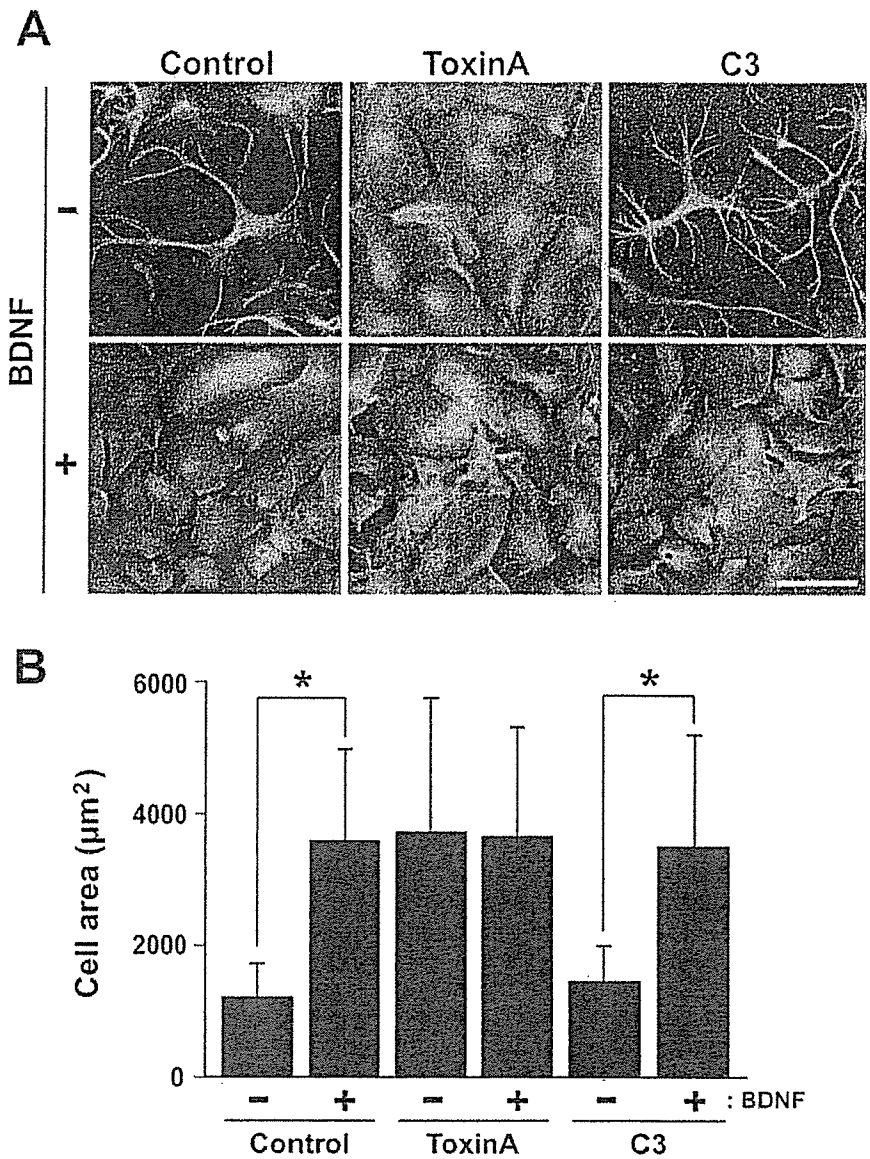

Figure 7. Morphological changes in astrocytes treated with Toxin A and C3 in 30 DIV astrocytic cultures. *A*, The images of cells treated by nothing (control), Toxin A, and C3. The 30 DIV astrocytes were incubated with Toxin A (20 ng/ml) or C3 (30 μg/ml) for 24 h. After being washed with serum-free medium, BDNF (20 ng/ml) was added to the cells, which were then fixed in 4% formaldehyde. The cells were stained with anti-T1 (green) and anti-GFAP (red). All displays show merged images (yellow). Scale bar, 50 μm. *B*, Quantitative analysis of cell size. Values are given as means ± SD of four independent experiments (total cell counts: control, without BDNF, $n = 914$, with BDNF, $n = 991$; Toxin A, without BDNF, $n = 948$, with BDNF, $n = 1064$; C3, without BDNF, $n = 1055$, with BDNF, $n = 1072$). The asterisks indicate statistically significant differences ($p < 0.05$; paired Student's *t* test).

Discussion

In the present study, we demonstrated that (1) a truncated TrkB receptor, T1, is capable of ligand-mediated signaling via Rho GDI1, which acts as a negative inhibitor in the Rho signaling cascade, and (2) the T1 signaling cascade regulates glial cellular morphology. A schematic representation is shown in Figure 10*C*. Our findings clearly indicate that T1 is not only the dominant-negative form of TK+, but is also the active receptor of BDNF itself.

Interaction between T1 and Rho GDI1

The *in vitro* binding analysis clearly showed the direct binding of Rho GDI1 and T1 (Fig. 2). One would question what fraction of T1 and Rho GDI1 contributes to the association between T1 and Rho GDI1. In the Western blot analysis in Figure 4, we loaded the 100 μg total protein per lane for TrkB, which is approximately one-third amount of total protein in each lysate derived from a 3 cm dish. As shown in Figure 4*A-C*, the level of the precipitated T1 in the control (at 0 min or no addition of BDNF) is comparable with the total level. In addition, in this study, the immunoprecipitations with anti-GDI or anti-pan-TrkB were performed with an efficiency of ~30%. The one-fourth of each precipitate was loaded on SDS-PAGE. Therefore, 44% of total T1 in an astrocyte bind to Rho GDI1.

In Figure 4*D*, ~1/60 amount of total protein in each lysate (5 μg total protein per lane) for Rho GDI1 was loaded on each lane. As described above about T1, we calculated the fraction of Rho GDI1 in the interaction between T1 and Rho GDI1. Consequently, ~2.2% of total Rho GDI1 in an astrocyte is involved in the binding to T1. It is a big surprise for us that the drastic change of astrocytic morphology is attributable to the low percentage of Rho GDI1 associating with T1. Rho GTPases are implicated in the important cell functions via remodeling cytoskeleton such as proliferation, migration, elongation of neurites, and membrane trafficking, suggesting that Rho GTPases are strictly regulated. Therefore, Rho GDI1 as a regulator of Rho GTPases are also severely controlled. Then, Rho GDI1 regulated by T1 may be small amount. A part of the rest of Rho GDI1 may be interacted with ERM consisting of ezrin, radixin, and moesin (Sasaki and Takai 1998) and might be bound to other unknown proteins.

Interaction between T1 and other proteins

p75 has been reported to control the activity of RhoA in a Rho GDI1-dependent manner (Yamashita et al., 1999; Yamashita and Tohyama, 2003). In the present study, we demonstrated that T1 also binds directly to Rho GDI1 and that LFH residues in the T1-specific sequence is important for this type of binding. Be-

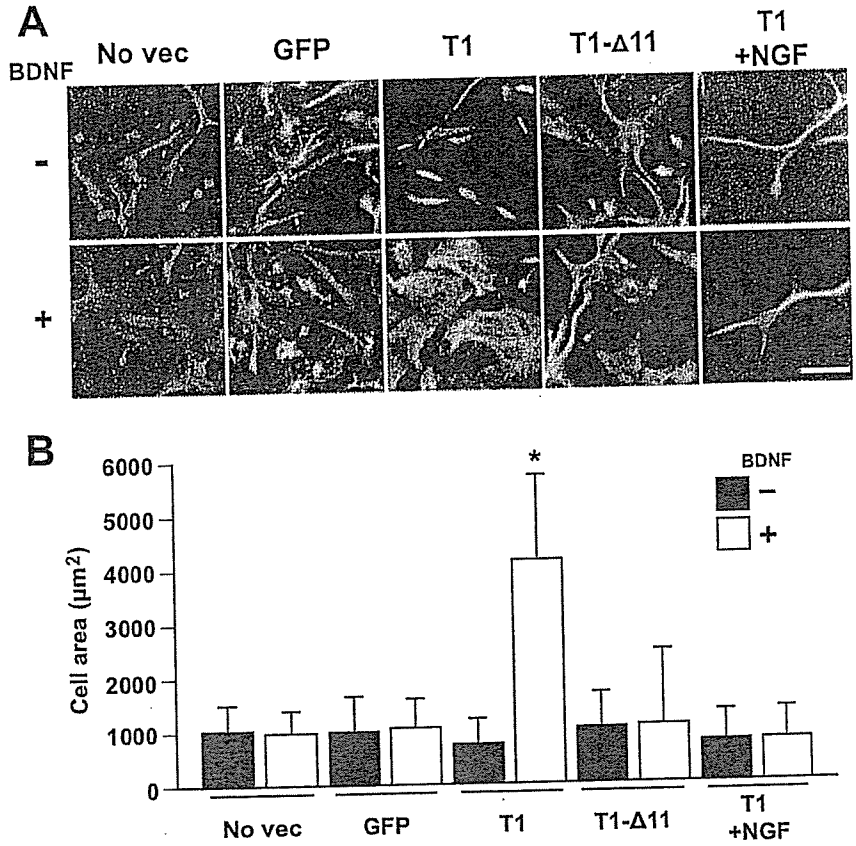

Figure 8. Morphological changes in astrocytes in 2 DIV cultures. *A*, No Vec, No transfection; GFP, EGFP; T1, normal T1; T1-Δ11, a deletion form of the T1-specific sequence (see Fig. 2*B*); T1 + NGF, normal T1-expressing cells that were treated with 100 ng/ml NGF instead of with BDNF. The cells were stimulated with vehicle (−) or with 20 ng/ml BDNF (+) and then were stained with anti-GFAP. Almost all of the cells were double positive for GFP (green) and GFAP (red), except for the No Vec cells. All displays show merged images (yellow-green). Scale bar, 30 μm. *B*, Quantification of cell size in *A*. Values are given as the means ± SD from the results of four independent experiments (total cell counts: No Vec, without BDNF, $n = 854$, with BDNF, $n = 821$; GFP, without BDNF, $n = 879$, with BDNF, $n = 787$; T1, without BDNF, $n = 698$, with BDNF, $n = 731$; T1-Δ11, without BDNF, $n = 687$, with BDNF, $n = 634$; T1 + NGF, without BDNF, $n = 810$, with BDNF, $n = 834$). The asterisks indicate significant differences ($p < 0.05$; one-way ANOVA and Scheffé's *post hoc* test) from the values obtained without BDNF treatment.

cause LFH is not contained in the intracellular domain of p75, both T1 and p75 may bind different regions of Rho GDI1.

Recently, Kryl and Barker (2000) reported that truncated TrkB-interacting protein (TTIP) is isolated from 15N neuroblastoma cells by using coimmunoprecipitation with GST fusion protein containing the intracellular juxtamembrane. TTIP has a molecular weight of 61 kDa, and T1 peptide competitively interrupted TTIP binding to T1, suggesting the direct binding interaction between them. However, the BDNF stimulation cannot modulate the interaction between T1 and TTIP. Kryl and Barker (2000) also analyzed TTIP by using matrix assisted laser desorption/ionization-mass spectrometry and described that TTIP is an unique protein. It is uncertain whether Rho GDI1 and TTIP bind directly to the different motifs in the T1-specific region or compete the same binding site. T1-mediated signaling may depend on its cellular compartment, because a fraction of T1 binds Rho GDI1. On the other hand, we detected proteins of 50, 60, and 72 kDa eluted from an affinity column (Fig. 1*A*); however, the correlation of each of these proteins with TTIP remains to be clarified.

Regulation of Rho proteins and astrocytic morphology by T1

The T1-interacting protein, Rho GDI1, is an inhibitory regulator of the Rho GTPases: Rho GDI1 is able to inhibit the activation of RhoA, Cdc42, and Rac1. On the other hand, the Rho GTPases are involved in the remodeling of the actin cytoskeleton: RhoA is involved in the formation of stress fibers; activated Cdc42 and Rac1 lead to lamellipodia and cell spreading, whereas activated Cdc42 induces filopodia (Hall, 1998). In this study, we demonstrated that Rho GDI1 released from T1 decreased the activities of the Rho GTPases, RhoA, Cdc42, and Rac1. However, it has remained unclear which Rho protein is related to the morphological changes in astrocytes triggered by BDNF. All Rho GTPases are known to be inhibited by Toxin A, and the form of astrocytes treated with Toxin A became flat. In contrast, the addition of C3, an inhibitor of RhoA, led to the formation of fibrous astrocytes with fine processes. Therefore, we were able to distinguish at least three types of morphology in this experiment. In the first type, the astrocytes became flat when all Rho GTPases were inhibited (Toxin A in Fig. 7*A*). In the second type, when only RhoA was inhibited by C3, the morphology of the cells was fibrous (C3 in Fig. 7*A*), which differed from the morphology of 30 DIV cells before the addition of BDNF (at 0 min in Fig. 5*A* and control in Fig. 7*A*), and the morphology of the fibrous cells also differed from that of T1-expressing 2 DIV cells (T1 in Fig. 8*A*). In the C3-treated condition, the processes of the astrocytes resembled filopodia; that is, fine processes extended from the bold processes of the astrocytes and the cell bodies (C3 in Fig. 7*A*). In the third type, the cells were not as fibrous as the second type of cell when the activities of the Rho GTPases remained at their basal levels. Typically, 30 DIV and T1-overexpressing astrocytes had spindle-shaped bodies or small, flat cell bodies and long processes (Figs. 5*A*, 7*A*, 8*A*). Thus, it appears that BDNF-T1 signaling suppressed the activity of all three Rho proteins and then induced morphological change leading to the flat type 1 cells. In addition, the cell flattening appears to be mediated primarily by the suppression of Cdc42 and Rac. In this context, it should be emphasized that extension of the astrocyte cell bodies was observed as a result of the inhibition of the Rho GTPases by T1-Rho GDI1 signaling. Recent studies have shown that the Rho GTPases control the remodeling of microfilaments, intermediate filaments, and microtubules (Ridley, 2001; Etienne-Manneville and Hall, 2002). Therefore, the regulation of cell morphology is not solely dependent on the microfilaments but instead depends on the well orchestrated control of various cytoskeletal proteins. More precise information regarding the mechanism of their regulation by BDNF remains to be obtained by additional study.

Functional role of T1 in astrocytes

In the present study, we demonstrated that astrocytes are able to alter their morphology rapidly and dramatically via the T1 > Rho GDI1 > Rho GTPase signaling cascade in a BDNF-dependent manner. In the mature mammalian CNS, BDNF is synthesized and secreted from presynaptic and/or postsynaptic sites, depend-

ing on neural activity (Fawcett et al., 1998; Aloyz et al., 1999; Hartmann et al., 2001; Kohara et al., 2001). Thus, astrocytic morphological changes might take place in an activity-dependent manner. On the other hand, recent studies have reported that glial morphology is drastically altered to maintain the clearance of neurotransmitters and to maintain the neural network and neural plasticity (Iino et al., 2001; Oliet et al., 2001; Hirrlinger et al., 2004). In addition, calcium entry into astrocytes has been assumed to be important for the modulation of synaptic transmission (Araque et al., 1999). More recently, T1 has been shown to mediate BDNF-induced calcium signaling in astrocytes (Rose et al., 2003; for review, see Kovalchuk et al., 2004). Although it remains unclear whether or not the entry of calcium into astrocytes can induce the alteration of astrocytic morphology, a mechanism involving the Rho GTPases might be associated with the entry of calcium into astrocytes (Illenberger et al., 1998; Ghisdal et al., 2003; Mehta et al., 2003). Thus, morphological changes attributable to the T1 signaling cascade in astrocytes surrounding synapses may modulate neuron–glial interactions as well as local calcium buffering effects, which would eventually lead to rapid changes in synaptic transmission. The relationship between the T1 signaling cascade and the entry of calcium into astrocytes appears to require additional examination.

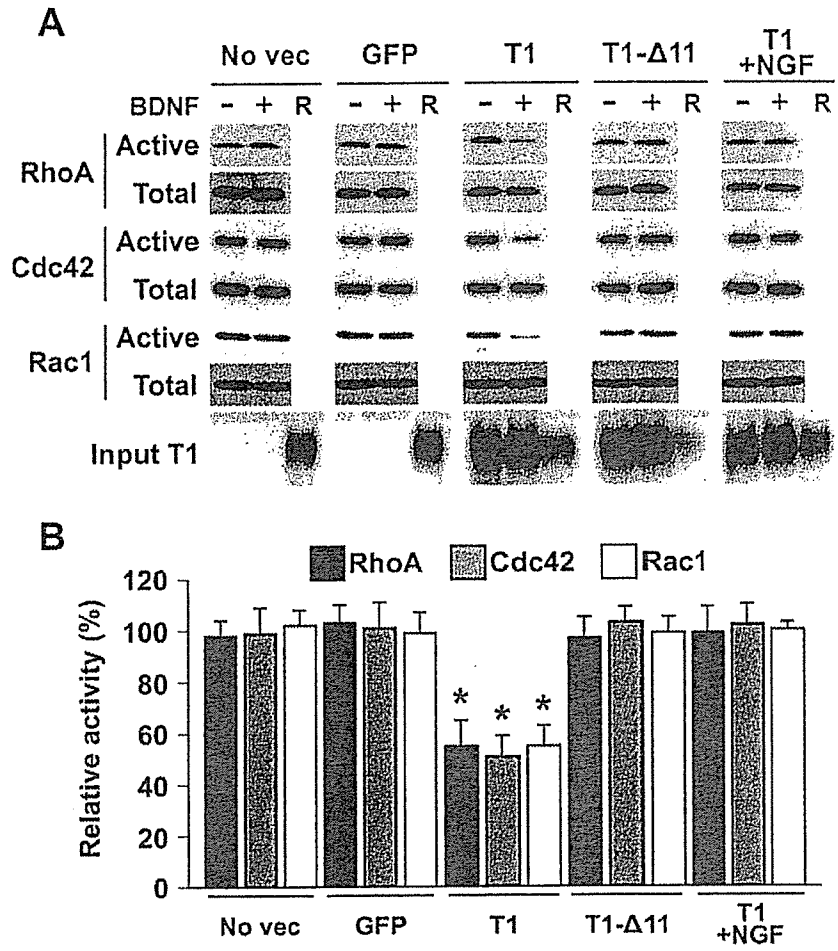

Figure 9. Activities of Rho GTPases in 2 DIV astrocytic cultures. *A*, No vec, No transfection; GFP, EGFP; T1, normal T1; T1-Δ11, a deletion form of T1 (see Fig. 1*C*); T1 + NGF, normal T1-expressing cells that were treated with 100 ng/ml NGF instead of BDNF. Cells were stimulated with vehicle (−) or with 20 ng/ml BDNF (+). The "R" in each column represents a rat brain sample. Overexpressed T1 and endogenous T1 from rat brain samples were detected by anti-T1 antibody, and overexpressed T1-Δ11 was detected by anti-pan-TrkB. Then, the precipitated proteins and total proteins (5 μg for RhoA; 100 μg for Cdc42 and Rac1) were loaded on 15% gel, and each protein was detected with a specific antibody. *B*, Quantitative analysis of Rho GTPase bands in *A*. Each control level, without BDNF stimulation, was taken as 100%. The asterisks indicate statistically significant differences ($p < 0.05$; paired Student's *t* test). Values are given as the means ± SD of four independent experiments.

References

Allendoerfer KL, Cabelli RJ, Escanòn E, Kaplan DR, Nikolics K, Shatz CJ (1994) Regulation of neurotrophin receptors during the maturation of the mammalian visual system. J Neurosci 14:1795–1811.

Aloyz R, Fawcett JP, Kaplan DR, Murphy RA, Miller FD (1999) Activity-dependent activation of TrkB neurotrophin receptors in the adult CNS. Learn Mem 6:216–231.

Araque A, Parpura V, Sanzgiri RP, Haydon PG (1999) Tripartite synapses: glia, the unacknowledged partner. Trends Neurosci 22:208–215.

Armanini MP, McMahon SB, Sutherland J, Shelton DL, Phillips HS (1995) Truncated and catalytic isoforms of trkB are co-expressed in neurons of rat and mouse CNS. Eur J Neurosci 7:1403–1409.

Barbacid M (1994) The Trk family of neurotrophin receptors. J Neurobiol 25:1386–1403.

Baxter GT, Radeke MJ, Kuo RC, Makrides V, Hinkle B, Hoang R, Medina-Selby A, Coit D, Valenzuela P, Feinstein SC (1997) Signal transduction mediated by the truncated trkB receptor isoforms, trkB.T1 and trkB.T2. J Neurosci 17:2683–2690.

Bibel M, Barde YA (2000) Neurotrophins: key regulators of cell fate and cell shapes in the vertebrate nervous system. Genes Dev 14:2919–2937.

Biffo S, Offenhäuser N, Carter BD, Barde YA (1995) Selective binding and internalization by truncated receptors restrict the availability of BDNF during development. Development 121:2461–2470.

Dechant G, Barde YA (1997) Signalling through the neurotrophin receptor $p75^{NTR}$. Curr Opin Neurobiol 7:413–418.

Eide FF, Vining ER, Eide BL, Zang K, Wang XY, Reichardt LF (1996) Naturally occurring truncated trkB receptors have dominant inhibitory effects on brain-derived neurotrophic factor signaling. J Neurosci 16:3123–3129.

Etienne-Manneville S, Hall A (2002) Rho GTPases in cell biology. Nature 420:629–635.

Fawcett JP, Bamji SX, Causing CG, Aloyz R, Ase AR, Reader TA, McLean JH, Miller FD (1998) Functional evidence that BDNF is an anterograde neuronal trophic factor in the CNS. J Neurosci 18:2808–2821.

Frisén J, Verge VM, Fried K, Risling M, Persson H, Trotter J, Hökfelt T, Lindholm D (1993) Characterization of glial trkB receptors: differential response to injury in the central and peripheral nervous systems. Proc Natl Acad Sci USA 90:4971–4975.

Fryer RH, Kaplan DR, Feinstein SC, Radeke MJ, Grayson DR, Kromer LF (1996) Developmental and mature expression of full-length and truncated TrkB receptors in the rat forebrain. J Comp Neurol 374:21–40.

Ghisdal P, Vandenberg G, Morel N (2003) Rho-dependent kinase is involved in agonist-activated calcium entry in rat arteries. J Physiol (Lond) 551:855–867.

Haapasalo A, Koponen E, Hoppe E, Wong G, Castrén E (2001) Truncated trkB.T1 is dominant negative inhibitor of trkB.TK+-mediated cell survival. Biochem Biophys Res Commun 280:1352–1358.

Hall A (1998) Rho GTPases and the actin cytoskeleton. Science 279:509–514.

Hartmann M, Heumann R, Lessmann V (2001) Synaptic secretion of BDNF after high-frequency stimulation of glutamatergic synapses. EMBO J 20:5887–5897.

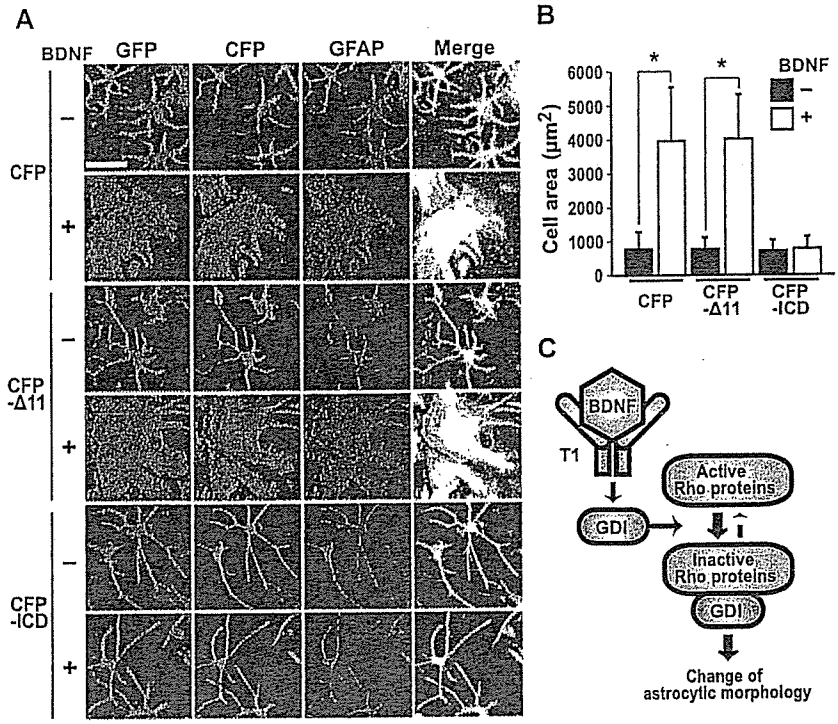

Figure 10. Competitive assay by overexpression of T1-specific C-terminal peptides. *A*, Expression vectors of T1 and CFP, CFP-Δ11, or CFP-ICD were cotransfected into astrocytes. CFP-Δ11 is a CFP-ICD lacking the 11 C-terminal amino acid residues. CFP-ICD is a fusion protein of CFP and the ICD segment of T1. The cells were stimulated with vehicle (−) or with 20 ng/ml BDNF (+). The cells with three overlapping colors are shown here in white. Scale bar, 50 μm. *B*, Quantification of each astrocytic area in *A*. Values are given as the means ± SD from the results of four independent experiments (total cell counts: CFP, without BDNF, $n = 859$, with BDNF, $n = 948$; CFP-Δ11, without BDNF, $n = 835$, with BDNF, $n = 960$; CFP-ICD, without BDNF, $n = 913$, with BDNF, $n = 955$). The asterisks indicate significant differences ($p < 0.05$; one-way ANOVA and Scheffé's *post hoc* test) from the values obtained without BDNF. C, Simplified schematic of the T1 signaling cascade. In astrocytes, the T1 signaling cascade acts as a negative inhibitor of the Rho GTPases in a BDNF-dependent manner, resulting in the morphological alteration of astrocytes. The bold lines indicate the signaling cascade promoted by BDNF. The broken lines indicate a lack of signal transduction.

Hirrlinger J, Hülsmann S, Kirchhoff F (2004) Astroglial processes show spontaneous motility at active synaptic terminals in situ. Eur J Neurosci 20:2235–2239.

Iino M, Goto K, Kakegawa W, Okado H, Sudo M, Ishiuchi S, Miwa A, Takayasu Y, Saito I, Tsuzuki K, Ozawa S (2001) Glia-synapse interaction through Ca^{2+}-permeable AMPA receptors in Bergmann glia. Science 292:926–929.

Illenberger D, Schwald F, Pimmer D, Binder W, Maier G, Dietrich A, Gierschik P (1998) Stimulation of phospholipase C-β_2 by the Rho GTPases Cdc42Hs and Rac1. EMBO J 17:6241–6249.

Just I, Selzer J, von Eichel-Streiber C, Aktories K (1995) The low molecular mass GTP-binding protein Rho is affected by toxin A from Clostridium difficile. J Clin Invest 95:1026–1031.

Kaplan DR, Miller FD (2000) Neurotrophin signal transduction in the nervous system. Curr Opin Neurobiol 10:381–391.

Klein R, Conway D, Parada LF, Barbacid M (1990) The *trkB* tyrosine kinase gene codes for a second neurogenic receptor that lacks the catalytic kinase domain. Cell 61:647–656.

Knüsel B, Rabin SJ, Hefti F, Kaplan DR (1994) Regulated neurotrophin receptor responsiveness during neuronal migration and early differentiation. J Neurosci 14:1542–1554.

Kohara K, Kitamura A, Morishima M, Tsumoto T (2001) Activity-dependent transfer of brain-derived neurotrophic factor to postsynaptic neurons. Science 291:2419–2423.

Kovalchuk Y, Holthoff K, Konnerth A (2004) Neurotrophin action on a rapid timescale. Curr Opin Neurobiol 14:558–563.

Kryl D, Barker PA (2000) TTIP is a novel protein that interacts with the truncated T1 TrkB neurotrophin receptor. Biochem Biophys Res Commun 279:925–930.

Maekawa M, Ishizaki T, Boku S, Watanabe N, Fujita A, Iwamatsu A, Obinata T, Ohashi K, Mizuno K, Narumiya S (1999) Signaling from Rho to the actin cytoskeleton through protein kinases ROCK and LIM-kinase. Science 285:895–898.

Mehta D, Ahmmed GU, Paria BC, Holinstat M, Voyno-Yasenetskaya T, Tiruppathi C, Minshall RD, Malik AB (2003) RhoA interaction with inositol 1,4,5-trisphosphate receptor and transient receptor potential channel-1 regulates Ca^{2+} entry. Role in signaling increased endothelial permeability. J Biol Chem 278:33492–33500.

Middlemas DS, Lindberg RA, Hunter T (1991) *trkB*, a neural receptor protein-tyrosine kinase: evidence for a full-length and two truncated receptors. Mol Cell Biol 11:143–153.

Offenhäuser N, Muzio V, Biffo S (2002) BDNF binding to truncated trkB.T1 does not affect gene expression. NeuroReport 13:1189–1193.

Ohira K, Hayashi M (2003) Expression of TrkB subtypes in the adult monkey cerebellar cortex. J Chem Neuroanat 25:175–183.

Ohira K, Shimizu K, Hayashi M (1999) Change of expression of full-length and truncated TrkBs in the developing monkey central nervous system. Brain Res Dev Brain Res 112:21–29.

Ohira K, Shimizu K, Hayashi M (2001) TrkB dimerization during development of the prefrontal cortex of the macaque. J Neurosci Res 65:463–469.

Oliet SHR, Piet R, Poulain DA (2001) Control of glutamate clearance and synapse efficacy by glial coverage of neurons. Science 292:923–926.

Ploug M, Jensen AL, Barkholt V (1989) Determination of amino acid compositions and NH_2-terminal sequences of peptides electroblotted onto PVDF membranes from tricine-SDS-PAGE: application to peptide mapping of human complement component C3. Anal Biochem 181:33–39.

Ren XD, Kiosses WB, Schwartz MA (1999) Regulation of the small GTP-binding protein Rho by cell adhesion and the cytoskeleton. EMBO J 18:578–585.

Ridley AJ (2001) Rho GTPases and cell migration. J Cell Sci 114:2713–2722.

Rose CR, Blum R, Pichler B, Lepier A, Kafitz KW, Konnerth A (2003) Truncated TrkB-T1 mediates neurotrophin-evoked calcium signalling in glia cells. Nature 426:74–78.

Sahara Y, Westbrook GL (1993) Modulation of calcium currents by a metabotropic glutamate receptor involves fast and slow kinetic components in cultured hippocampal neurons. J Neurosci 13:3041–3050.

Sasaki T, Takai Y (1998) The Rho small G protein family-Rho GDI system as a temporal and spatial determinant for cytoskeletal control. Biochem Biophys Res Commun 245:641–645.

Shelton DL, Sutherland J, Gripp J, Camerato T, Armanini MP, Phillips HS, Carroll K, Spencer SD, Levinson AD (1995) Human trks: molecular cloning, tissue distribution, and expression of extracellular domain immunoadhesins. J Neurosci 15:477–491.

Takai Y, Sasaki T, Matozaki T (2001) Small GTP-binding proteins. Physiol Rev 81:153–208.

Thoenen H (2000) Neurotrophins and activity-dependent plasticity. Prog Brain Res 128:183–191.

Yacoubian TA, Lo DC (2000) Truncated and full-length TrkB receptors regulate distinct modes of dendritic growth. Nat Neurosci 3:342–349.

Yamashita T, Tohyama M (2003) The p75 receptor acts as a displacement factor that releases Rho from Rho-GDI. Nat Neurosci 6:461–467.

Yamashita T, Tucker KL, Barde YA (1999) Neurotrophin binding to the p75 receptor modulates Rho activity and axonal outgrowth. Neuron 24:585–593.